Possible evidence for variation in magnitude for marsquakes from fallen boulder populations, Grjota Valles, Mars

Jason. R. Brown, Gerald. P. Roberts,

Department of Earth and Planetary Sciences, Birkbeck, University of London, WC1E 7HX, United Kingdom

Abstract

Following observations of mobilized boulder trail populations from Cerberus Fossae, Mars, that have been interpreted as possible evidence of large magnitude marsquakes rupturing for distances of ~207 km along exposed active faults, additional boulder trail populations were measured along shorter faults within the region of Grjota Valles (50-150 km length) to test the hypotheses that (1) these faults are also candidate locations for marsquakes, and (2) that marsquake magnitude might be smaller, limited by fault dimensions available for rupture. For a region containing two en echelon graben, boulder trail data define two anomalies with maxima in (a) boulder trails per kilometer, and (b) maximum width of boulder trails, one that is ~116 km in length along strike and the other ~70 km in length along strike. Values for the maxima are 45 trails per km and 5 m mean trail width for the 70 km long anomaly, and 115 trails per km with 5.3 m mean trail width for the 116 km long anomaly, above background values measured elsewhere along these faults of zero trails per kilometer with zero boulder trail widths. If combined with published data from Cerberus Fossae with a ~207 km long anomaly in boulder trails per km (125 trails per km maxima) and maximum mean boulder trail width (8.5 m maximum trail width), the 3 datasets suggest correlations between the (a) along-strike length of boulder trail anomalies, (b) boulder trails per km and (c) maximum boulder trail width. If interpreted as due to single marsquakes, and if the dimensions of these anomalies are a proxy for rupture length, when combined, one interpretation of this is that boulders have been mobilized by marsquakes and that the marsquake magnitude is proportional to the along strike length of the anomalies. In other words, the data suggest that marsquake magnitude, if that is the cause of the anomalies, is limited by fault length as expected for terrestrial seismically active faults. Such findings suggest that the Martian surface may have been shaken, in the very recent past, by large magnitude marsquakes. We discuss this in terms of the seismicity of Mars.

1 Introduction

Given that the diameter of Mars (6,790 km) is much smaller than that of the Earth (12,750 km) it has long been considered that Mars is less geologically active than the Earth because the internal heat source for volcanism and associated faulting would have been lost more quickly (see Roberts et al. 2012 for a discussion). However, studies by Antoine et al. (2010) suggest that endogenic heat sources might well be present within Mars associated with the Cerberus Fossae fault system. Roberts et al. (2012), using understanding of natural seismometers on Earth, suggested that large magnitude marsquakes may have occurred in the recent past along Cerberus Fossae, evidenced by observations close to faults of anomalies in the density of trails left by mobilized boulders and boulder trail widths (Figs. 1 and 2). Roberts et al. (2012) showed, for Cerberus Fossae, that boulder trail densities per kilometre and boulder trail widths increased systematically from background values along the strike of part of the fault system, interpreting this as possible evidence that a marsquake had produced ground shaking responsible for mobilization of the boulders. This study was facilitated by the advent of HiRISE imagery (High Resolution Imaging Science Experiment onboard the Mars Reconnaissance Orbiter) whose high resolution (~25 cm pixel sizes) allowed, for the first time, observations of boulders and boulder trails from orbit, in particular the largest boulders and trails, and hence the ability to map the characteristics of boulder populations along the strike of fault systems. Roberts et al. (2012) suggested that boulder populations mobilized by seismic shaking, in particular the widest boulder trails, would show decreases in mobilized boulder frequency and boulder size over tens of kilometres or more away from putative epicentres if produced by single large events, as observed on the Earth (Fig. 1), and evidenced on Mars by the widths of trails in dust left by mobilized boulders. In contrast, boulder populations mobilised by processes facilitating release of boulders from steep cliffs, such as melting of ground ice on steep slopes, would produce spatially uniform boulder trail populations, lacking anomalies with dimensions of tens of kilometres or more. Measurements presented by Roberts et al. (2012) were consistent only with the hypothesis of mobilisation by seismic shaking (Fig. 1). Furthermore, the trails in the underlying sediment left by boulders as they rolled and bounced down slopes suggests relatively-recent boulder mobilization and hence possible ongoing marsquake activity. This is because tracks produced by the rovers Spirit and Opportunity were erased over

timescales of only days to months (Geissler et al. 2010), due to the passage of dust storms during the perihelion season, although evidence exists of track preservation for longer periods of time in locations sheltered from the wind; thus tracks left by boulders would also be erased, suggesting that preserved examples must be relatively young if the material is fine enough to be mobilised by the wind. Tracks produced by boulders at Cerberus Fossae are wider and deeper (several meters, several decimeters) than trails left by rovers (centimetres, centimetres to millimetres) so presumably it would take longer to erase them with aeolian processes, but the same arguments apply and it is difficult to envisage an age as old as, for example, 10^6 – 10^7 years for the boulder trails. Roberts et al. (2012) also pointed out that the geographic dimension of the boulder trail width/frequency anomaly, along the strike of the fault system, might be indicative of the magnitude of the marsquake, as is the case on Earth (Keefer 1984). The ~207 km wide zone of mobilized boulders measured along Cerberus Fossae might be consistent with a marsquake of moment magnitude ~M7.9 (see Wells and Coppersmith 1994). A marsquake of this magnitude is not inconsistent with the along strike extent of the faults of Cerberus Fossae because Vetterlein and Roberts (2009) showed that these faults exhibit continuous along-strike displacement profiles constraining a fault length of ~325 km, longer than the implied rupture extent, although Knapmeyer et al. (2006) suggested a maximum magnitude of 7.6. Vetterlein and Roberts (2010) showed that the dmax/length (measured as vertical offset, throw, in this example) of the Cerberus Fossae faults was ~0.1-0.001, similar to those measured on Earth, suggesting that the relationships between slip dimensions and marsquake magnitude might also be similar to the Earth. The question that arises is whether other examples exist on Mars where shorter fault lengths are associated with smaller along-strike extents of boulder trail anomalies, implying smaller moment magnitudes.

In this paper we seek to extend our knowledge of possible marsquakes by investigating whether: (a) other possible examples of boulder trail anomalies can be identified, with evidence ruling out causes other than marsquakes for their formation, and (b) whether marsquakes of different magnitudes and hence different epicentral shaking intensities to mobilise boulders can be inferred. To this end we have studied another set of faults that are parallel to the southern Cerberus Fossae faults located in the region of Grjota Valles (Fig. 2). Faults in the vicinity of Grjota Valles offset: (i) planar surfaces that are probably lava flows, (ii) inliers of older terrain such as hills that protrude upwards through the lava flows, and (iii) outflow channels that may be of aqueous or volcanic origin associated with

volcanism (e.g. Burr et al. 2003, Plescia 2003, Jaeger et al. 2010, Morgan et al. 2013, Hamilton 2013 for associated examples). This means that the Grjota Valles faults are very similar morphologically to those along Cerberus Fossae studied by Roberts et al. (2012). Like the examples from Cerberus Fossae described by Roberts et al. (2012), initial inspection of down faulted regions in Grjota Valles examples revealed many thousands of boulder trails made by mobilised boulders that have fallen from fault-controlled cliffs (Figure 3). However, it is clear from inspection of imagery that the faults associated with Grjota Valles are segmented (Fig. 2), with segments that are shorter (maximum of 60-80 km) than those associated with Cerberus Fossae (Vetterlein and Roberts 2009, 2010; Taylor et al. 2013). This combination of features allows us to test: (a) whether anomalies in boulder trail densities and dimensions occur along the faults and are best explained by marsquakes, and (b) if they are best explained by marsquakes, whether their dimensions correlate with the dimensions of fault segments. To this end, we examined all the HiRISE images (Figures 2 and 3) that were available at the time of the study, to constrain the extent of boulder trail anomalies; see Fig. 2 b, c & Fig. 2 a). We explain in detail why we have separated the faults into Boulder Trail Anomaly 1 and Boulder Trail Anomaly 2, based on boulder trail data, below. We have identified two local maxima in boulder trail densities (that also correlate with boulder trail width) – one associated with each fault line. We discuss these in terms of their most likely mode of formation, concluding that marsquakes may be the most likely cause. We then discuss the results in terms of the possible occurrence of marsquakes with magnitudes controlled by fault dimensions, while also considering that the marsquake activity may well be relatively recent.

First, we present maps of the fault system containing two en echelon graben/faults, one which is ~115 km length along strike and the other ~82 km length along strike (Figs. 2, 3 and 4). Secondly, we present data concerning the density of boulder trails per kilometer and boulder trail widths. After discussing the cause of the boulder trail anomalies, concluding that marsquakes may be the most likely cause of the boulder trail results, and explaining why other causes are unlikely, we conclude that with the two new boulder trail data sets presented in this paper, and the example from Roberts et al. (2012), we have 3 examples where boulder trail anomaly dimensions correlate with fault lengths and by analogy maximum along-strike rupture extent. Thus, the boulder trail data appear to be consistent with the interpretation that the boulders were mobilized by seismic shaking produced by marsquakes, and that boulder-trail data may help reveal the magnitudes of the marsquakes.

2 Geological Background

The fault system we study is located in the vicinity of Grjota Valles and comprises a ~197 km long set of en echelon graben segments located between latitude N16°10’33, longitude E160°33’48, and latitude N15°12’10 / longitude E163°40’00. The WNW-ESE orientation of the graben means that the fractures are sub-radial to the Elysium Mons volcano (Fig. 2 a), and may be the surface expression of sub-surface dikes. Detailed geological and geomorphological mapping reveals that the geometry of the faults is consistent with that of graben, with fault controlled cliffs adjacent to flat-bottomed depressions (Figs. 3, 4 and 5). MOLA data (Mars Orbiter Laser Altimeter on the Mars Global Surveyor (MGS) spacecraft) reveal that the vertical offset across the graben, which are exposed on a surface that slopes from -2100 m elevation to -2400 m elevation from west to east, increases form zero at the tips of the graben to ~900 m at latitude E162^{o} (Fig. 5). This reveals an offset/subsidence profile that is typical of faults, with vertical offsets as high as ~900 m, and a dmax/length ratio (with dmax measured as vertical offset for this example) for the whole structure of 0.005, within the range measured for terrestrial faults and those on Mars (Schlische et al. 1996; Vetterlein and Roberts 2010). In detail, the MOLA data constrain the vertical offset across the graben at 180 locations, and reveal displacement gradients and dmax/length ratios associated with individual distal and medial fault segments of 0.008-0.026, again similar to values measured on Earth (Vetterlein and Roberts 2010; Fig. 5). The similarity in dmax/length values between faults in Grjota Valles and the Earth suggest that the material strength is similar in the two regions (Gomez-Rivas et al. 2015). If the material strength is similar then the relationships between rupture length, dmax, stress drop and moment magnitude are also likely to be similar (Ali and Shieh 2013). Thus, our dmax/length observations support the suggestion that these are faults formed by similar deformation processes to those on the Earth and it may be possible to infer some aspects of the seismicity, such as moment magnitude, from observations of surface deformation.

The faults can be shown to be relatively recent in that they crosscut pre-existing features of known, relatively-young age (Fig. 2 and 4). The fossae offset Late Amazonian Cerberus lavas and older inliers (Tanaka et al. 2005). It is believed that the ages of the youngest lavas offset on the nearby Cerberus Fossae, assessed by crater counting methods, are <10 Ma (Head et al. 2003; Hartmann and Berman,; 2000; Vaucher et al. 2006), implying

that the fossae, if they are all approximately the same age, are even younger. The ~900 m offset revealed by MOLA data (Fig. 5), if developed since 10 Ma as implied by crater-count ages, implies a rate of vertical offset of ~0.09 mm/yr, a value that is similar to well-documented rift systems on the Earth (Vetterlein and Roberts 2010). The faults also offset a variety of geomorphic features such as lava plains, older inliers and outflow channels with stream-lined islands (Figure 2; Burr et al. 2003, Plescia 2003, Jaeger et al. 2010). The similar features were reported for the faults along Cerberus Fossae (Roberts et al. 2012), so we suggest a similar mode and age of formation for the faults in Grjota Valles.

3 Method

We mapped parts of the Grjota Valles fault system in detail to ascertain the nature of the geology of the region and gain an overview of the geomorphic features that the boulders were associated with (Fig. 4).

NASA HiRISE images have been accessed using the Planetary Data System (PDS) node at the University of Arizona (http://hirise.lplarizona.edu/) (Table 1). They were downloaded at their highest resolution. The images were imported into Google Earth as geo-referenced image overlays. At the time of writing, there were eighteen areas covered by HiRISE imagery within the study area of the Grjota Valles (Fig. 2). However, six of the locations are covered by two HiRISE images, and one of the images (ESP_027345_1955) covers an area which has 6 fractures, 2 of which were required for this study – meaning 12 images were used in total, with one (ESP_027345_1955) split into two images: 6a and 6b. We believe that the number of images available provide sufficient along-strike coverage of the structures for our purposes. The ruler tool in Google Earth was used to measure distances and hence boulder trail lengths and widths, allowing for boulder trail density to be calculated. Roberts et al. (2012) showed that such measurements reproduce the dimensions of ground-truthed terrestrial boulders to an extent that is adequate for our purposes. We also checked distance measurements in ArcGIS, and found that this provides values that are similar to the values from Google Earth to an extent that does not affect our conclusions (<1% difference between ArcGIS and Google Earth at the latitudes we are interested in).

We defined the width of boulder trails as the width between what we term “raised levees” or “sharp edges” that formed as the boulder traversed across the underlying substrate (Figure 3 a, b, c and d). We included boulder trails without terminal boulders. We measure the width of the trail where the trail is widest to exclude measurements where the boulder was bouncing and leaving a narrower trail. There is cross-image variation in boulder trail density on HiRISE images. Where one can see the substrate is coarse grained, with visible boulders, no trails exist. Examples of cross-trail variation are shown in Figure 3 b and c. Thus, we measured the distance across areas where we could gain continuous records on regions where the substrate appeared fine-grained, converting the values into number per kilometer.

For each HiRISE image we measured the following:

1) We recorded the location of every boulder trail that we were able to identify in each of the 13 areas along c. 1.5 km – 6.5 km long transects along the slopes immediately adjacent to the floors of the graben. (e.g. Fig. 6). These transects were chosen because (i) they existed at the bases of steep slopes along fault-controlled cliffs, and (ii) fine-grained deposits (probably aeolian sand and dust) were present that preserved boulder trails. We did not make measurements where the surface was formed of coarse-grained sediments (> ~20-50 cm particle size) or on solid rock because such locations would be unlikely to preserve the passage of mobilized boulders if such motion had occurred. The zig-zag lines in Figure 6 show (a) that we proceeded in a general along strike direction, not returning to along strike locations where we had already noted boulder trails, because we were concerned that this could result in erroneous double-counting of boulder trails in our inventory, and (b) the exact locations where we measured boulder trail width (blue dots), in general the widest part of the trail, so we could revisit the locations of measurements at a later date if needed. Along strike distance was recorded as the longitude of each blue dot on Figure 6, for conversion into the values of boulder trails per kilometer in Figure 8 using trigonometry and a conversion factor for degrees longitude into kilometers. In summary, the along-track lengths of the zig-zag tracks were not used in any calculation, but serve to record exactly how we traversed the boulder trail population and exactly where we made measurements. We are confident that we have measured every boulder trail where densities were relatively low (< ~45 boulder trails per km) because they were clear on the imagery. However, in places it was difficult to recognize every individual boulder trail at higher densities because some boulder trails coalesce; in these locations (> ~45 boulder

trails per km) we think we may have underestimated the number of boulder trails per km, but this does not affect our overall conclusions (e.g. Fig. 6, with results in Figs. 7 and 8). We also note that if the boulder trails were < ~95 cm in width they would not have been resolved on current imagery, so again this may have lead us to underestimate the boulder trail density, but again this does not affect our conclusions as our hypothesis depends on the largest mobilised and hence the widest boulders trails (Fig. 1).

2) We measured the width of the 10 widest boulder trails we could identify in each image, reporting the mean value, to provide an estimate of the dimensions of mobilized boulders.

We were aware that measuring distances using a ruler tool in software on pixellated images can be subjective so the two authors made independent measurements of the same images, with Figure 7a and 7b showing comparisons between results from the two authors. These results show that the results are repeatable with results from the two surveys being broadly comparable within error. The differences between results from the two authors (< 1m for the mean value for the 10 widest boulder trails; <10-20 boulder trail counts per km) are far smaller than the signals that were measured (between 1 and 5.5 m for the mean value for the 10 widest boulder trails; between 0 and 100 for the boulder trail counts per km). Overall, we are confident that our method for measuring the number of boulder trails and their widths using the ruler tool in Google Earth is robust and repeatable if others were to make measurements from the same images.

4 Results

The data in Figure 8 shows that there are coincident maxima in boulder trail density and boulder trail widths along the strike of the faults in Grjota Valles.

In terms of the spatial variations in boulder trail density along the strike of the fault system, maxima in boulder trail counts exist at around E161.5° and E162.5° longitude. Boulder trail count values decrease both east and west from these locations along the strike of the faults towards their lateral terminations. We use these variations to define Boulder Trail Anomaly 1 and Boulder Trail Anomaly 2 mentioned above and shown in Figure 2c. For Boulder Trail Anomaly 2 we measured a peak of 45 boulder trail counts per km at E161.43° longitude, with lower values recorded closer to the east and west tips of the

graben. For Boulder Trail Anomaly 1, a peak of 102 counts per km at E162.03° was measured, again with lower values recorded closer to the east and west tips of the graben.

We note that values for boulder trails per km exhibit an asymmetric pattern along strike (Fig. 8 a and b). The westernmost point of Boulder Trail Anomaly 2 exhibits the smallest number of trails per km at 5 trails per km at E160.57° longitude, with the number of trails increasing as we follow the fault east, culminating in a peak of 45 counts per km at E161.43° longitude. This is followed by a sharp decrease in the number of recorded trails, with 4 per km at E161.74° longitude, giving the graph in Figure 8 an asymmetric appearance. For Boulder Trail Anomaly 1, measurements begin at E161.76° longitude, extremely close to the tip of Boulder Trail Anomaly 2, but at a latitude of N15.81°, some 6 km to the south of the last measured point along Boulder Trail Anomaly 2. The first count along Boulder Trail Anomaly 1 records 30 counts per km at E161.7° followed by a sharp increase in counts, rising to a peak of 102 counts per km at E162.03° longitude, the highest count along the entire fault. Further east the number of counts decreases, dropping to 2 counts per km at E163.63° close to the lateral termination of Boulder Trail Anomaly 1. Again, these measurements give an asymmetric shape (Fig. 8 b).

Coincident with boulder trail counts per km, there are maxima in boulder trails widths, with mean values again increasing from close to zero near tips of the structures towards maximum values (Figs. 8a and 8c). This shows that the areas of high boulder trail density also have the widest boulder trails (compare Figs. 8b and 8c). Again we note an asymmetry along strike of the graben for the boulder trail width data. The widest mean boulder trail width along Boulder Trail Anomaly 2 was ~5 m, and this measurement was recorded in the region exhibiting the highest number of boulder trails at E161.43° longitude. As with boulder trails per km, a sharp decrease in the mean width of boulder trails is observed as we progress west along the fault, with a mean trail width of 1.4 m being recorded in the region where only four boulder trails were located (E161.76°). Boulder Trail Anomaly 1 also clearly exhibits the aforementioned relationship, with a maximum mean boulder trail width of ~ 5 m located in the area of most boulder trails per km (102), and from this peak the mean width of trails drops to 1.7 m at E163.62°, an area where only 2 boulder trails per km were recorded (Fig. 8d). Note that for Boulder Trail Anomaly 1, both the boulder trail width and boulder counts per kilometer, if extrapolated along strike, have maximum values near to longitude E162.5^{o}, a location where the surface expression of the fault appears to be non-existent due to the presence of tips to

individual graben (see Fig. 2 b, c); a flat plain separates two graben at this location, and we discuss the possible reasons for this later in the paper. We also note that there does not appear to be an obvious correlation between the vertical offset across the graben and the number of boulder trails per km or the mean value for the size of the 10 widest boulder trails (see locations A and B in Figure 8); again this is discussed later in the paper.

5 Discussion

Results from Grjota Valles show geographically coincident maxima in boulder trail density per km and boulder trail widths along the graben. This type of observation was used by Roberts et al. (2012) to suggest that the most plausible mechanism to mobilize such populations of boulders is seismic shaking associated with palaeomarsquakes (see Figure 1). They concluded this because boulders mobilized by seismic shaking would "display the classic pattern associated with earthquakes where both the frequency of boulder falls and boulder sizes decrease away from the epicenter and the location of coseismic surface faulting, due to localized ground shaking (Keefer 1984)" (Fig. 1). However, there are other possible mechanisms that may have mobilised the boulders, and we discuss each of them in turn below.

1) *Release of boulders by melting ice.* A plausible hypothesis is that boulders are held on the steep slopes and cliffs associated with the graben by water or CO_2 ice. Any diurnal, seasonal or longer-term warming might melt the ice and release the boulders. Roberts et al. (2012) suggest that boulders mobilized in this way would show "a random spatial pattern of maximum boulder sizes" when sampled over "tens to hundreds of kilometers" (Figure 1). However, our measurements show clear local maxima in boulder trail widths and boulder trail density per kilometer that are geographically coincident (Figure 8). Note, the actual mean value for the widest boulder trail may be larger if measured from a larger population of trails, so there is an element of circular reasoning here. However, even with this caveat, these results, with geographically-coincident maxima in values for the two variables (Figure 8), are not what would be expected of the mechanism of boulder release by melting ice. Furthermore, it is unclear how this process could control the dimensions of boulders recorded by the boulder trail widths, and, like Roberts et al. (2012), (their Figure 10), we have found no evidence for differing joint-spacing in the bedrock to explain the variable maximum boulder sizes implied by the variable maximum boulder trail widths, although the restriction of image resolution means we cannot rule it out. Furthermore,

349 persistent CO_2 frost may not be plausible at this latitude (Piqueux et al., 2016), so it may
350 be unrealistic to expect such frost to hold boulders on slopes. For these reasons so we
351 reject this hypothesis.
352
353 2) *The effect of local differences lithology and hence weathering/erosion.* A plausible
354 hypothesis is that different lithologies might be more or less prone to erosion and this
355 might control the number and sizes of boulders released from the steep slopes and cliffs
356 associated with the graben. Our geological mapping shows no obvious changes in
357 lithology of the rocks forming the walls to graben (Figure 4). We have also examined
358 available THEMIS (Thermal Emission Imaging System) and CRISM (Compact
359 Reconnaissance Imaging Spectrometer for Mars) data to try to ascertain if local lithological
360 changes correlate with the measured maxima in boulder trail widths that are coincident
361 with the measured maxima in boulder trails per kilometer. The CRISM data, although
362 having limited lateral extent and hence availability, appear to show no obvious change in
363 lithology of the rocks forming the walls to graben with regard to oxidised iron minerals,
364 mafic mineralogy, hydroxylated silicates, bound water or water ice and CO_2 ice
365 (Supplementary Figure S1). The THEMIS data, including both night time and daytime
366 infrared measurements, provide complete spatial coverage of the area studied, and,
367 although probably saturated in the images we show, again show no obvious change in
368 lithology of the rocks forming the walls to the graben, highlighting only that the walls of the
369 graben appear to formed of bedrock (Supplementary Figures S2 and S3), as confirmed by
370 the clear stratigraphic layers in the HiRISE images (Figure 4). The HiRISE data show a
371 layered stratigraphy in the graben walls that are presumably lava flows and possibly
372 sedimentary layers formed by weathering erosion and aeolian processes between lava
373 flow events. There appears to be little if any obvious differences in stratigraphy between
374 different HiRISE images (Figure 4). Thus, as we have not identified any changes in
375 lithology, despite having a variety of data sources, we reject the hypothesis that different
376 lithologies might be more or less prone to erosion and this might control the number and
377 sizes of boulders released from the steep slopes and cliffs associated with the graben. We
378 also have no evidence to address the possibility that that wind helps dislodge rocks, either
379 directly or by forcing sand and dust into cracks, wedging them open, in a way that
380 produces the regional variations in boulder trail frequency and size shown in Figure 8.
381
382 3) *Higher cliffs could supply more boulders.* A plausible hypothesis is that the higher
383 frequency of boulder trails we have measured in some HiRISE images might be explained

by proximity to higher cliffs that have a greater number of loose boulders available for mobilization. However, it is not just the cliffs that supply boulders. The talus at the bases of the cliffs also contains boulders that could be mobilised as they are likely to be sitting on slopes that are close to their angle of repose. Thus, the combined height of the cliffs and the talus should be taken into account. Also, the talus slopes are all likely to be close to their angle of repose, and the cliffs appear to be close to vertical, so variations in local slope is probably not a variable that needs to be considered. Although it is not possible to measure the heights and slopes of all the individual cliffs or individual talus cones, because (a) MOLA spot spacing of ~300 m is too coarse (Supplementary Figure S4), (b) shadow width and solar incidence angle cannot be used to define vertical height differences via trigonometry, because the horizontal extents of talus slopes vary between different examples (Supplementary Figure S5), and (c) stereo HiRISE pairs to make local digital elevation models are not available for the majority of HiRISE locations in the study area, it is possible to measure the total offset across the faults controlling the graben walls using the MOLA data (Figures 5 and 8). For example, locations A and B in Figure 8 show similar values for boulder trails per kilometer and boulder trail widths, but very different combined heights of the fault-controlled cliffs plus talus slope height defined by the total offset measured with MOLA data. Thus, if the vertical extent of cliffs plus associated talus slopes provides more candidate boulders for mobilization, this does not tally with our measurements of maxima in boulder trail frequency. Also, this hypothesis does not explain why the widths of boulder trails correlate with the frequency of boulder trails. Thus, for these two reasons we reject this hypothesis.

4) *Boulder mobilization caused by nearby impacts.* A plausible hypothesis is that formation of nearby impact craters could have produced ground shaking that mobilized the boulders. We have examined all impact craters within ~ 50 km across strike of the graben we have studied. A ~4 km diameter crater is located at Latitude 15.618^{o} and Longitude 162.183^{o}, close to the area with maxima in boulder trail frequency and boulder trail width. However, the ejecta blanket from this crater has been eroded by an outflow channel, so the crater pre-dates the outflow. The outflow channels pre-date the graben evidenced by cross-cutting relationships (see Vetterlein and Roberts 2009 for a description of how cross-cutting relationships are ascertained), and the boulder trails post-date graben formation. Hence, this crater is too old to have been involved in boulder mobilization. Smaller craters (~ 40 m diameter) exist within a few hundred metres of the graben in the vicinity of the maxima in boulder trail frequency and width (Supplementary Figure S6). However, these

craters, although having a relatively young appearance at first sight, due to the existence of dark, presumably relatively dust-free material within them, are in fact partially filled with aeolian dunes. The dunes were mobilized by the wind, yet the boulder trails have not been destroyed by the action of wind, suggesting that they are younger than the dunes. Thus, if the rate of aeolian processes is similar between these craters and the graben floors, these small craters are also ruled out as candidates for producing the ground shaking that mobilized the boulders. Thus, as no candidate craters have been identified we rule out this hypothesis, but note that this is dependent on our assumption that the rate of aeolian processes is similar between craters and the graben floors.

5) *Track density may correlate with better preservation and/or lower degradation rather than more abundant formation.* A plausible hypothesis is that the boulder trails may be degraded by erosion, and that degradation may vary spatially influencing the number of trails that are preserved, and the widths that are measured. To assess this we have compared boulder trail widths with the dimensions of the boulders that formed them (Figure 3 d). We assume that the boulders are more resistant to wind erosion than the underlying dust surfaces that they have rolled over, and will maintain their original dimensions. Thus, a comparison between the dimensions of the boulders and the trails should reveal whether trail widths have been altered by wind erosion. We have found that in areas of both high and low boulder trail density and width, the widths of the boulder trails are indistinguishable in width from the width of the boulders that formed them. This suggests the trails are not eroded to an extent that radically alters their widths or preservation. That the trails have not been significantly degraded by wind erosion is consistent with the preservation of raised levees produced by the motion of boulders, evidenced by variation in percentage grayscale for individual pixels in the images (Figure 3 d (v)). Thus, we reject this hypothesis.

6) *Variation in incidence angle of the images makes trails difficult to see.* A plausible hypothesis is that recognition of trails may be hindered by, for example, the solar incidence angles in the HiRISE images. Supplementary Figure S7 shows that solar incidence angles are very similar for the images we have studied. Also, our qualitative assessment after studying many examples is that individual boulder trails are as clear on images with low boulder trail frequency and width as they are on images with high boulder trail frequency and width. For these reasons we reject this hypothesis.

7) *The accumulation of boulder trail populations may have developed from multiple single rock falls through time.* As single rockfalls have been observed on repeat imagery (for example see https://www.msss.com/mars_images/moc/2005/09/20/bouldertracks/ which appears to show possible bounce marks and longer lived debris flow channels) then a plausible hypothesis is that repeated single rock-falls could be responsible for the populations of boulder trails, perhaps triggered by many small marsquakes or many releases of boulder by melting ice or other processes. Our qualitative observation on this point is that the morphology of the boulder trails appears to be identical across the many thousands of boulder trails we have observed. They appear to have raised levees only a few decimetres across that are presumably made of dust to coarse sand (Figure 3 d). We think it is dust to coarse sand because it is susceptible to being disturbed by a rolling boulder to form a raised levee, and hence we also think it would be susceptible to subsequent wind erosion (Figure 3 d). We do not think these examples on Mars are associated with gravel-grade material that would be less susceptible to wind erosion. This is because we have conducted fieldwork in Iceland where boulder trails have formed in talus cones on fault scarps made of gravel-grade material (grain size of up to 10-15 cm) (Supplementary Figure S8). The examples in Iceland lack raised levees and we think this is due to the relatively-coarse grain-size, and hence interpret the grainsize for the examples from Mars as dust to coarse sand. The raised levees in the examples from Mars are, as described above, evidenced by variation in percentage grayscale for individual pixels in the images with the sun illuminating the raised levees that also produce shadows (Figure 3 d). The key point is that with clear examples of active aeolian processes on the graben floors in the form dunes (e.g. Figure 4 a), and the interpreted dust to coarse sand grainsize, the fact that raised levees are preserved in many thousands of examples suggests they are young and hence of very similar age. For this reason we reject the hypothesis of incremental formation of the boulder trail populations by addition of single boulder falls, although we admit that this is supported only by qualitative observations. Rather, we suggest that two events have formed the two boulder trail populations shown in Figure 8. Note that if we are incorrect about the levees, and in fact the population of boulder trails contains examples of individual boulder trails with very different ages, then the population could have accumulated through many smaller rock falls, invalidating our large magnitude marsquake interpretations, but we suggest that our evidence appears to point to the opposite interpretation, consistent with large magnitude marsquakes.

8) *Measurements used to define boulder trail anomalies.* A plausible hypothesis is that

there may be a problem with our measurements. It may be that the mean width of the 10 widest trails is inadequate to allow comparison of boulder trail populations produced by mobilization of a sub-set of the population of available boulders, if populations of different number are considered and they have a power-law or exponential size distribution. One scenario could be that if more are boulders are drawn from such a population, there will be more individual large boulders and the mean will be larger, even if the size-frequency distribution is identical. We have been unable to define the number, as we have not counted the total number of boulders in each location, but it is perhaps likely that the extremely large numbers of candidate boulders for mobilization at every location means that the population sizes are not significantly different. Our results stand if we assume that the number of boulders in the population is identical between locations, but clearly we have not been able to rule out this possibility.

After consideration of the alternative scenarios described above, we conclude, following Roberts et al. (2012), that a plausible explanation for the boulder trail data we present herein may be that the boulders were mobilized by seismic shaking associated with palaeomarsquakes, with shaking, and hence boulder mobilization, decreasing with distance from the epicentres. Thus, although, perhaps not completely proven, as we have not ruled out some alternative hypotheses, we think it worthwhile to explore the implications that arise if this marsquake hypothesis is correct.

We note that the marsquake interpretation requires one of our interpreted marsquake ruptures to cross an area where there is no surface offset. We note that it is common for ruptures to jump between active faults that are not physically continuous in terrestrial earthquakes and provide an example of this in Supplementary Figure S9 (see Livio et al. 2016). The same may apply on Mars. This is important to note, because, like on the Earth, estimates of maximum marsquake magnitude may be erroneously small if it is assumed that ruptures can be confined to single active faults.

If our conclusion that the boulder populations were mobilized by marsquakes is correct, the observation that the results of this study are similar to those of Roberts et al. (2012), suggests that we should discuss data from that paper alongside those in this paper to broaden our understanding of the potential significance of the boulder trail populations (Fig. 9). An obvious difference between the data sets is that the hump-shaped anomalies extend over ~207 km for Cerberus Fossae (Roberts et al. (2012), whilst those that emerge

524 from this paper extend over ~116 km for Boulder Trail Anomaly 1, and ~70 km for Boulder
525 Trail Anomaly 2 (Fig. 9). Roberts et al. (2012) suggested that the along strike extent of
526 seismic shaking great enough to mobilise boulders on Earth is approximately the same as
527 the along strike extent of surface faulting for the earthquake ruptures, consistent with
528 observations from the 2009 Mw 6.3 earthquake near L'Aquila, Italy. Roberts et al. (2012)
529 also tentatively mapped possible surface rupture extent using HiRISE images for Cerberus
530 Fossae, and observations were consistent with the hypothesis. Following this, although we
531 have not been able to map rupture extent in the present example, and the 1:1 ratio
532 between rupture length and the dimensions of areas with mobilized boulders on Earth is
533 only approximate, if the along strike extent of the hump-shaped anomalies in boulder trail
534 data are taken as proxies for along strike rupture extent, the implied moment magnitudes
535 for the palaeomarsquakes, assuming that the humps result from single events, may be in
536 the range of ~Mw 7.3-7.8 (Fig. 9d). It should be noted that our assumption that the
537 anomalies formed in single events and not multiple small events (see the discussion in
538 Point 7 above), mean that these magnitudes should be considered as maximum values.
539 However, our assumptions are supported indirectly by the observation that dmax/length
540 ratios for the Martian faults examined herein (0.026-0.008; Figure 5) are similar to those
541 measured on the Earth (0.1-0.001; see Vetterlein and Roberts 2010 for a review). In turn,
542 this implies that material strength and the relationships between rupture length, dmax,
543 stress drop and moment magnitude are also likely to be similar to those on the Earth
544 (Gomez-Rivas et al. 2015; Ali and Shieh 2013). Moment magnitudes in the range of ~Mw
545 7.3-7.8 implies events whose seismic shaking would be widely felt/detected on the Martian
546 surface by seismometers such as those associated with the Interior Exploration using
547 Seismic Investigations, Geodesy and Heat Transport (InSIGHT) mission. However, also
548 note that we may be mistaken in our assumption that along strike extent of the hump-
549 shaped anomalies in boulder trail data is a proxy for along strike rupture extent, as
550 unfortunately, unlike Roberts et al. (2012), we have been unable to map surface rupture
551 for example in Grjota Valles. Gravity on Mars is ~38% compared to that of the Earth so
552 less force might be needed to mobilise boulders, but it is hard to be precise as this
553 depends on how each boulder was attached and detached, and whether each boulder was
554 mobilized by vertical or horizontal accelerations (see Supplementary Figure S5 c-h for an
555 explanation). However, it is possible that the along strike extent of the hump-shaped
556 anomalies in boulder trail data may be greater than along strike rupture extent, so this is
557 another reason why the estimates of ~Mw 7.3-7.8 should be considered maximum values.
558 Nonetheless, if we use the observation that boulder trail anomalies have similar along

559 strike dimensions to suggested surface ruptures for the Cerberus Fossae example
560 (Roberts et al. 2012), the results point towards the conclusion that a variety of magnitudes
561 of palaeomarsquake may have been detected, with larger magnitudes on the Cerberus
562 Fossae fault system which displays fault segments lengths of several hundred kilometers
563 from geomorphic observations of offset features, and smaller magnitudes on the Grjota
564 Valles system where segmented lengths are in the range of 50-100 km, again from
565 geomorphic observations (Fig. 2 and Fig. 9). This correlation between fault dimensions
566 and dimensions of areas affected by putative seismic shaking adds further support, albeit
567 indirect, for our interpretation of palaeomarsquakes.
568
569 Furthermore, we suggest that it may be possible to infer details of how well seismic
570 shaking is recorded by our natural seismometer, that is, the boulder trail population data.
571 Fig. 10a compares the three faults; Boulder Trail Anomaly 1, Boulder Trail Anomaly 2 and
572 Roberts et al.'s (2012) fault, plotting boulder trails per km versus boulder trail width. A
573 positive relationship exists between boulder trails per km and the width of boulder trails,
574 with a greater number of boulder trails corresponding to a greater width of boulder trails.
575 However, it is interesting to note that the data appear to saturate. Data from Roberts et al.
576 (2012) increase from zero to ~5-8 m for the mean value of the 10 widest boulder trails over
577 the range of ~0-50 boulder trails per km, and then appear to flatten out at larger values
578 with the value of ~5-8 m for the mean value of the 10 widest boulder trails maintained over
579 the range of ~50-125 boulder trails per km. One interpretation of this is that the natural
580 seismometer is saturating, and unable to record shaking that would mobilise larger
581 boulders. It may be that boulders > 5 - 8 m are not available in great numbers on the fault-
582 controlled slopes, perhaps controlled by joint spacing or layer thicknesses in the rocks.
583 Furthermore, we note that the Fig. 10 b shows a positive relationship between the along
584 strike length of the boulder trail anomaly and the maximum value for boulder trails per km
585 recorded. This may be interpreted to suggest that maximum ground acceleration may
586 increase with marsquake magnitude. However, we note that from the sparse data we
587 have, constrained with only 3 data points, that the trend again flattens-out, and that we
588 might expect the example from Roberts et al. (2012) to have more than the ~120 boulder
589 trails per km recorded. We suggest that again the natural seismometer might be
590 saturating, perhaps because once a value of ~45 boulder trails per km is exceeded it
591 becomes difficult in some cases to identify every single boulder trail because they appear
592 to coalesce on the images. The preceding text pertaining to performance of our natural
593 seismometer is speculative. However, we note that if correct, it implies that boulder trail

populations may not be effective in measuring the effects of marsquakes at the largest magnitudes because the measurements may be saturated.

As a final point of discussion we note that profiles of data for boulder trail anomalies 1 and 2 are asymmetric (Figures 8 and 9), with the steepest gradients closest to the en echelon fault step-over (labelled A in Figure 9a) between these two fault segments. For faults on the Earth we note that displacement gradients steepen in the step-over zones between interacting faults (Jackson et al. 2002). The asymmetry in boulder trails populations may, perhaps, be related to this. A speculative interpretation might be that slip-distributions for each of the individual marsquake ruptures that produced these boulder-trail anomalies were skewed towards the tips of fault segments, so that the largest coseismic displacements, and hence highest levels of ground acceleration, were located close to the en echelon step-over between the fault segments, as occurs on the Earth (Faure Walker et al. 2009).

Overall, the boulder trail data presented in this paper are intriguing, but not conclusive. Clearly, what is needed is for a seismometer placed on the surface of Mars to actually record a marsquake before we can conclude that seismicity is present (see Lorenz et al. 2017 who suggest that seismometer data from the Viking missions may have already detected seismic shaking, and data acquisition planned for the InSIGHT seismometer mission to Mars of 2018-19). The data herein may suggest relatively large events, perhaps up to Mw 7.3-7.8. However, magnitudes >Mw 7.6 seems improbable given the analysis of Knapmeyer et al. (2006). We point out that the uncertainty indicated by the spread in the data supporting Figure 9d allow our interpretation to be consistent with the estimate in Knapmeyer et al. (2006). Nonetheless, events as large Mw 7.6 would have recurrence intervals that are very long (perhaps hundreds to thousands of years), much longer than the lifetime of a seismometer. The likelihood of measuring such an event with the InSIGHT seismometers is, of course, very small. However, if like on the Earth, for every large event there are hundreds to thousands of smaller events with shorter return times following Gutenberg-Richter b-value scaling (e.g. Knapmeyer et al. 2006), it may be that one of these smaller events is more likely to be recorded by the InSIGHT seismometers.. The annual detectability of such events by the InSIGHT instruments was investigated by Taylor et al. (2013), and they conclude that between 1.5×10^0 and 1.9×10^5 events would be detected, depending on the maximum defined event size; our results provide new information on the possible maximum event sizes. The ideas in this paper can and should

be tested by data provided by the InSIGHT mission. The data in this paper suggest that the Martian surface is not completely still; instead they hint that the Martian surface may well have be shaken by large magnitude marsquakes in the very recent past.

6 Conclusions

We have studied two faulted areas in the vicinity of Grjota Valles (Boulder Trail Anomaly 1 and Boulder Trail Anomaly 2), measuring the densities and widths of boulder trails created by boulders falling from fault-controlled cliffs. These data are consistent with previous results (Roberts et al. 2012) in that the most parsimonious interpretation is that boulders have been mobilized by seismic shaking associated with palaeomarsquakes in the recent past. Our conclusions can be tested with data from the InSIGHT mission that is on the Martian surface at the time of writing. For now, we report that a region containing two en echelon graben/faults with similar dmax/length ratios to those from the Earth, boulder trail data define two maxima in (a) boulder trails per kilometer and (b) maximum width of boulder trails, one which is ~116 km length and the other ~70 km length. Values for the maxima are 45 trails per km and 5 m maximum trail width for the 70 km long anomaly, and 115 trails per km with 5.3 m maximum trail widths for the 116 km long anomaly, above background values of zero trails per kilometer with zero boulder trail widths. Combined with published data from Cerberus Fossae where the a ~207 km long anomaly in boulder trails per km (125 trails per km maxima) and maximum boulder trail width (8.5 m maximum trail width), the 3 datasets suggest correlations between the along-strike length of boulder trail anomalies, boulder trails per km and maximum boulder trail width. Implied moment magnitudes, derived by using the along strike dimensions of boulder trail anomalies as proxies for rupture extent, could be as large as Mw 7.3-7.8, values that we expect to be accompanied by much more frequent seismic activity at lower moment magnitudes.

Acknowledgements

We acknowledge STFC grant ST/K006037/1 that funded some of this work. We acknowledge the HiRISE teams (NASA/JPL/University of Arizona) for providing images and the MOLA team for topographic data. We thank Jonny Roberts for his help with the fieldwork in Iceland. The data used in this paper are appropriately cited in the references section of this paper. We thank the reviewers and Associate Editor for their detailed and constructive comments.

663

664 **References**

665

666 Ali, W., Shieh, S, (2013) Earthquake repeat time, stress drop, type of slip and earthquake
667 magnitude. J. Geol. Geosci., 2:2. http://dx.doi.org/10.4172/2329-6755.1000118

668 Antoine, R., T. Lopez, D. Baratoux, M. Rabinowicz, K. Kurita, (2010) Thermal analysis of
669 fractures at Cerberus Fossae, Mars: Detection of air convection in the porous debris
670 apron. *Icarus, 214 (2):* 433-446.

671 Berman, D. C. and Hartmann W. K. (2002) Recent fluvial, volcanic, and tectonic activity on
672 the Cerberus Plains of Mars. *Icarus 159,* 1-17.

673 Burr, D.M., J. A. Grier, A. S. McEwen, L. P. Keszthelyi, (2002) Repeated aqueous flooding
674 from the Cerberus Fossae: Evidence for very recently extant, deep groundwater on
675 Mars. *Icarus 159:* 53-77.

676 Burr, D. M., A. S. McEwen, S. E. H. Sakimoto (2002) Recent aqueous floods from the
677 Cerberus Fossae, Mars. *Geophysical Research Letters 29 (1):* 13-1-13-4.

678 Faure Walker J., G.P. Roberts, P.A. Cowie, I. Papanikolaou, A.M. Michetti, P. Sammonds
679 and R. Phillips (2009) Horizontal strain-rates and throw-rates across breached relay-
680 zones, central Italy: implications for the preservation of throw deficits at points of
681 normal fault linkage. *Journal of Structural Geology,* 31, 1145-1160,
682 doi:10.1016/j.jsg.2009.06.01

683 Geissler, P. E., R. Sullivan, M. Golombek, J. R. Johnson, K. Herkenhoff, N. Bridges, A.
684 Vaughan, J. Maki, T. Parker, J. Bell (2010) Gone with the wind: Eolian erasure of the
685 Mars Rover tracks. *Journal of Geophysical Research: 115.*

686 Gomez-Rivas, E., Griera, A., Llorens, M.-G. (2015) Fracturing of ductile anisotropic
687 multilayers: influence of material strength. Solid Earth, 6, 497-514, 2015
688 https://doi.org/10.5194/se-6-497-2015.

689 Hamilton, C. W., Flood lavas associated with the Cerberus Fossa 2 unit in Elysium Planita,
690 Mars. (2013) Abstract for the 44th Lunar and Planetary Science Conference.

691 Hartmann, W. K. and Berman D. C. (2000) Elysium Planitia lava flows: Crater count
692 chronology and geological implications. *Journal of Geophysical Research 105 (E6):*
693 15011-15,025.

694 Head, J.W., L. Wilson, K. L. Mitchel (2003), Generation of recent massive water floods at
695 Cerberus Fossae, Mars by dike emplacement, cryospheric cracking, and confined
696 aquifer groundwater release. *Geophysical Research Letters 30 (11).*

Jackson, C. A. L., R. L. Gawthorpe, I. R. Sharp (2002) Growth and linkage of the East Tanka fault zone, Suez rift: structural style and syn-rift stratigraphic response. *Journal of the Geological Society. 159:* 175-187.

Jaeger, W. L., Keszthelyi, K. P., Skinner, J. A., Milazzo, M. P., McEwen, A. S., Titus, T. N., Rosiek, M. R., Galuszka, D. M., Howington-Kraus, E., Kirk, R. L., and HIRISE Team, (2010), Emplacement of the youngest flood lava on Mars: a short turbulent story. Icarus, 205, 230-243, doe:10.1016/j.icarus.2009.09.011.

Keefer D. K. (1984) Landslides caused by earthquakes. *Geological Society of America Bulletin. 95:* 406-421.

Knapmeyer, M., Oberst, J., Hauber, E., Wahlisch, M., Deuchler, C., Wagner, R. (2006) Working models for spatial distribution and level of Mars' seismicity. Journal of Geophysical Research, Vol. 111, E11006, doe10.1029/2006JE002708,

Livio F; Michetti AM; Vittori E; Gregory L**;** Wedmore L; Piccardi L; Tondi E; Roberts G; Blumetti AM; Bonadeo L; Brunamonte F; Comerci V; Di Manna P; Ferrario MF; Faure Walker J; Frigerio C; Fumanti F; Guerrieri L; Iezzi F; Leoni G; McCaffrey K; Mildon Z; Phillips R; Rhodes E; Walters RJ; Wilkinson M (2016) Surface faulting during the August 24, 2016, central Italy earthquake (Mw 6.0): Preliminary results, *Annals of Geophysics*, **59**, . doi: 10.4401/ag-7197

Lorenz, R. D., Nakamura, Y., Murphy, J. R. (2017) Viking-2 Seismometer Measurements on Mars: PDS Data Archive and Meteorological Applications. Earth and Space Science, 4, 11, p681-688.

Morgan, G., Campbell, B. A., Carter, L. M., Plaut, J. J., Phillips, R. J., (2013), 3D reconstruction of the source and scale of buried young flood channels on Mars. Science, 340, doi: 10.1126/sceince.1234787.

Piqueux, S., A. Kleinböhl, P. O. Hayne, N. G. Heavens, D. M. Kass, D. J. McCleese, J. T. Schofield, and J. H. Shirley (2016), Discovery of a widespread low-latitude diurnal CO2 frost cycle on Mars, J. Geophys. Res. Planets, 121, 1174–1189, doi:10.1002/2016JE005034.

Plescia, J. B. (2003) Cerberus Fossae, Elysium, Mars: a source for lava and water. *Icarus: 164:* 79-95.

Roberts, G.P., B. Matthews, C. Bristow, L. Guerrieri, J. Vetterlein (2012) Possible evidence of paleomarsquakes from fallen boulder populations, Cerberus Fossae, Mars. *Journal of Geophysical Research, 117*.

Schlische, R. W., S. S. Young, R. V. Ackermann, A. Gupta (1996) Geometry and scaling relations of a population of very small rift-related normal faults: *Geology, 24:* 683-686.

Tanaka, K. L., J. A. Skinner, T. M. Hare, (2005) Geologic Map of the Northern Plains of Mars. *Pamphlet to accompany Scientific Investigations Map 2888, USGS for NASA. https://pubs.usgs.gov/sim/2005/2888/.*

Taylor, J., Teanby, N. A., Wookey, J., (2013), Estimates of seismic activity in the Cerberus Fossae region of Mars, Journal of Geophysical Research, Planets, VOL. 118, 2570-2581, doi:10.1002/2013JE004469.

Vaucher, J., D. Baratoux, N.Mangold, P. Pinet, K. Kurita, M. Gregoire, (2009) The volcanic history of central Elysium Planitia: Implications for Martian magmatism. *Icarus, 204:* 418-422.

Vetterlein, J. and Roberts, G. P. (2009) Postdating of flow in Athabasca Valles by faulting of the Cerberus Fossae, Elysium Planitia, Mars. *Journal of Geophysics Research.*

Vetterlein, J. and Roberts, G. P. (2010) Structural Evolution of the Northern Cerberus Fossae graben system, Elysium Planitia, Mars. *Journal of Structural Geology, 32:* 394-406.

Wells, D. L. and Coppersmith, K. J. (1994) New empirical relationships among magnitude, rupture length, rupture width, rupture area, and surface displacement. *Bulletin of the Seismological Society of America, 84, (4):* 974-1002.

Figure Captions

Figure 1. Hypotheses to explain the characteristics of the widest examples of boulder trails formed by the mobilised boulder populations due to seismic shaking and release of boulders from cliffs by melting of ice. (a) Alternative hypotheses explored by Roberts et al. (2012). (b) Terrestrial rockfalls triggered by an earthquake. (c) Data from Roberts et al. (2012) for comparison with data presented in this paper.

Figure 2. Location maps**. (a)** MOLA images of Mars showing the location of the study area. **(b)** NASA image mosaic (visible imagery) with the location of the study area shown. The four white squares show the locations of the four geological and geomorphological interpretations for Images 1, 3, 9 and 12 (see Figure 4 (a), (b), (c) & (d)). **(c)** Map showing location of the studied boulder trail anomalies. Boulder Trail Anomaly 1 (red) and Boulder Trail Anomaly 2 (green) and location of HiRISE image footprints across the study area, numbered in accordance with number scheme used in this study. HiRISE images 1 through 13 were used in this study. (d) and (e) show details of the fault geometries and geomorphology and are located in (c) .

Figure 3. (a) Images showing typical locations and attributes of the boulder trails counted in this study. **(b) and (c)** A selection of images showing the variation in boulder trails between different HiRISE images and different parts of the same HiRISE images. (i) original image, with added white arrows pointing out a selection of boulder trails/bounce marks; (ii) the image with the boulder trail/bounce marks drawn in black, and (iii) with only the black infill. The figures illustrate only a small proportion of the total number of boulder trails in each image. **(d)** Observations of boulder trails and boulder dimensions. The similarity between the dimensions of boulders and boulder trails suggest that boulder trails have not been significantly affected by erosion.
(i) A possible hypothesis is that boulder trails may be degraded by erosion, and that degradation may vary spatially, influencing the number of trails that are preserved, and the widths that are measured. (ii) and (iii) Comparison of boulder trail widths with the dimensions of the boulders that formed them from ESP_026712_1960 and from ESP_025156_1965). (iv) Location map showing the position of ESP_026712_1960 and ESP_025156_1965. (v) That the trails have not been significantly degraded by wind erosion is consistent with the preservation of raised levees produced by the motion of boulders, evidenced by variation in percentage grayscale for individual pixels in the images. This is evidenced by visual inspection of many examples, and also evidenced by the percentage grayscale measurements we have made that show systematic variation in percentage grayscale on the floors of the tracks, not constant values as would be expected for a flat, depositional surface illuminated by the sun. If the levees are made of sand, and their preservation potential is low, then the ages of the boulder trails whose widths are defined by the levees is likely to be similar, and relatively young. In other words, the widespread preservation of levee crests in the images suggests the boulder trails are similar in age, because they have not been eroded/degraded. And that is what we use to suggest the population of boulder trails is mostly composed of individual trails of similar age, hence possibly produced in single, widespread events, that is, marsquakes.

Figure 4. (a), **(b)**, **(c)** & **(d)** Geological and geomorphological interpretations of Images 1, 3, 9 and 12. The geology/geomorphology on the fossae is that of a low-relief plain that has been faulted by graben structures, down-dropping central blocks that have been covered by colluvium and aeolian material.

Figure 5. The relationship between the map trace of the graben and vertical offsets constrained by MOLA data. **(a)** Plot of longitude against vertical offset measured across the south side of the graben from MOLA data. **(b)** CTX mosaic showing how the vertical offsets in (a) relate to the map geometry of the graben. **(c)** The location of MOLA data in latitude and longitude, showing how the vertical offsets in (a) relate to the map geometry of the graben. **(d)** Plot showing absolute values of elevation for the plain to the south of the graben, the plain north of the graben, and the floor of the graben, versus longitude.

Figure 6. Example of a boulder trail density measurement for two images: **(a)** Image 4 (HiRISE Image ESP_025011_1965) and **(b)** Image 8 (HiRISE Image ESP_026712_1960). **(a).** Image 4 (**a. (i)**) shows a sparse concentration of narrow trails, all of similar width and similar length. **a. (ii)** Blue dots at the apex of the dark lines indicate boulder trails along a transect shown in dark blue. **a. (iii)** Graph showing location and density of boulder trails found along a WNW-WSE transect traversing 0.03° of longitude, showing the locations of trails. **(b)**. Image 8 (**b. (i)**) shows a dense concentration of both narrow and some wider trails. The lengths of the trails in the image are comparable. Some trails exhibit bounce marks. **b. (ii)** Dots at the apex of the dark lines indicate boulder trails along a transect shown in dark blue. **b. (iii)** Graph showing location and density of boulder trails found along a WNW-WSE transect traversing 0.05° of longitude, showing the locations of trails.

Figure 7. Both authors counted boulder trails and boulder widths along Boulder Trail Anomaly 1 and Boulder Trail Anomaly 2. **(a)** Calibration graph for boulder trail counts. **(b)** Calibration graph for boulder width counts. Both of these results show that the results are repeatable with results from the two surveys being broadly comparable.

Figure 8. (a) Plot showing absolute values of elevation for the plain to the south of the graben, the plain north of the graben, and the floor of the graben, versus longitude. (b) Graph of longitude versus boulder trails per kilometer. (c) Graph of longitude versus boulder trails widths.

Figure 9. (a) Comparison of three data sets of boulder trails per kilometer against longitude for Boulder Trail Anomaly 1, Boulder Trail Anomaly 2 and data from Cerberus Fossae (Roberts et al. (2012)). Roberts et al. (2012) suggested that if the along strike extent of seismic shaking great enough to mobilize boulders on Earth is approximately the same as the along strike extent of surface faulting for the earthquake ruptures, it may be

836 possible to infer the magnitude of seismic events. Following this, if the long strike extent of
837 the hump-shaped anomalies in boulder trail data are taken as proxies for along strike
838 rupture extent, the implied moment magnitudes for the palaeomarsquakes, assuming that
839 the humps result from single events, is in the range of Mw 7.3-7.8. **(b)** Comparison of three
840 data sets of boulder trail density per kilometer against longitude for Boulder Trail Anomaly
841 1, Boulder Trail Anomaly 2 and data from Cerberus Fossae (Roberts et al. (2012)). **(c)**
842 Comparison of three data sets of ten widest boulder trails per kilometer against longitude
843 for Boulder Trail Anomaly 1, Boulder Trail Anomaly 2 and data from Cerberus Fossae
844 (Roberts et al. (2012)). **(d)** Graph of surface rupture length versus moment magnitude
845 adapted from Wells and Coppersmith (1994). If the long strike extent of the hump-shaped
846 anomalies seen in Figure 9 a-c in boulder trail data are taken as proxies for along strike
847 rupture extent, the implied moment magnitudes for the palaeomarsquakes, assuming that
848 the humps result from single events, is in the range of Mw 7.3-7.8.
849
850 **Figure 10. (a)** Comparison of three data sets of the ten widest boulder trails against
851 boulder trails per kilometer for Boulder Trail Anomaly 1, Boulder Trail Anomaly 2 and data
852 from Cerberus Fossae (Roberts et al. (2012)). **(b)** Comparison of three data sets of the
853 maximum number of boulder trails per kilometer against length of boulder trail anomaly for
854 Boulder Trail Anomaly 1, Boulder Trail Anomaly 2 and data from Cerberus Fossae
855 (Roberts et al. (2012)). Note the positive correlation between the along strike length of the
856 boulder trail anomaly and the maximum value for boulder trails per km recorded. This may
857 be interpreted to suggest that maximum ground acceleration may increase with
858 earthquake magnitude.
859
860 **Table1 HiRISE image observations used.**
861

Image number used in this paper	**HiRISE Image Name**	**Latitude (centered)**	**Longitude (East)**	**Map Projected Scale**
1	PSP_008502_1965	16.250°	160.575°	25 cm / pixel
2	ESP_018774_1965	16.085°	160.723°	50 cm / pixel
3	PSP_006999_1965	16.100°	160.828°	25 cm / pixel
4	ESP_025011_1965	16.141°	161.011°	25 cm / pixel
5	ESP_018708_1960	15.819°	161.448°	50 cm / pixel
6a	ESP_027345	15.571°	161.792°	50 cm /

	_1955			pixel
6b	ESP_027345_1955	15.571°	161.792°	50 cm / pixel
8	ESP_026712_1960	15.715°	162.013°	25 cm / pixel
9	PSP_006287_1955	15.479°	162.677°	25 cm / pixel
10	ESP_018075_1955	15.386°	162.928°	25 cm / pixel
11	ESP_028400_1955	15.329°	163.242°	25 cm / pixel
12	PSP_010361_1955	15.311°	163.336°	25 cm / pixel
13	PSP_007790_1955	15.209°	163.657°	25 cm / pixel

862

Figure 1

a) Hypothesis

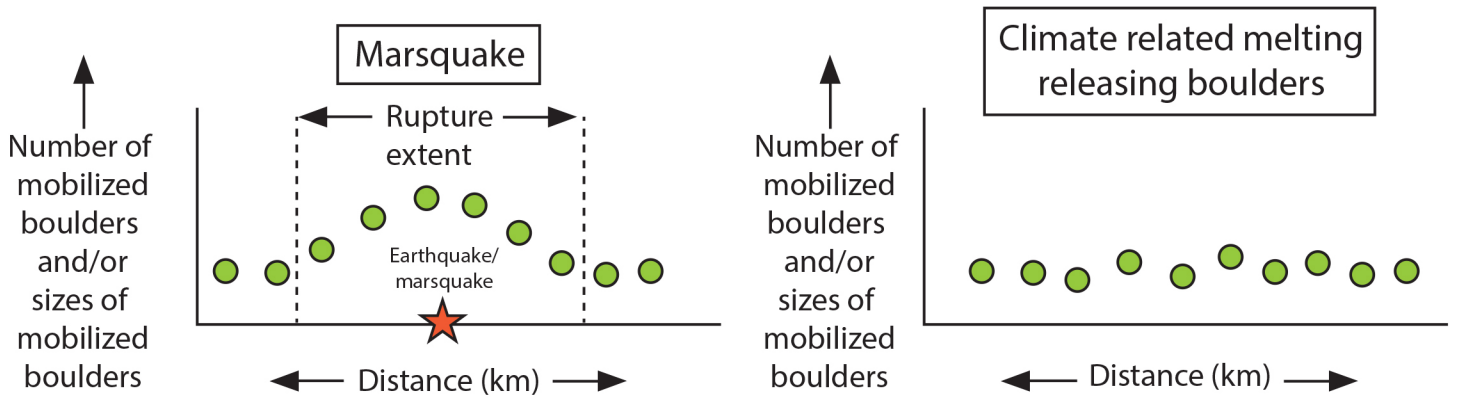

b) Terrestrial dataset - 2009 Mw 6.3 Earthquake, L'Aquila, Italy

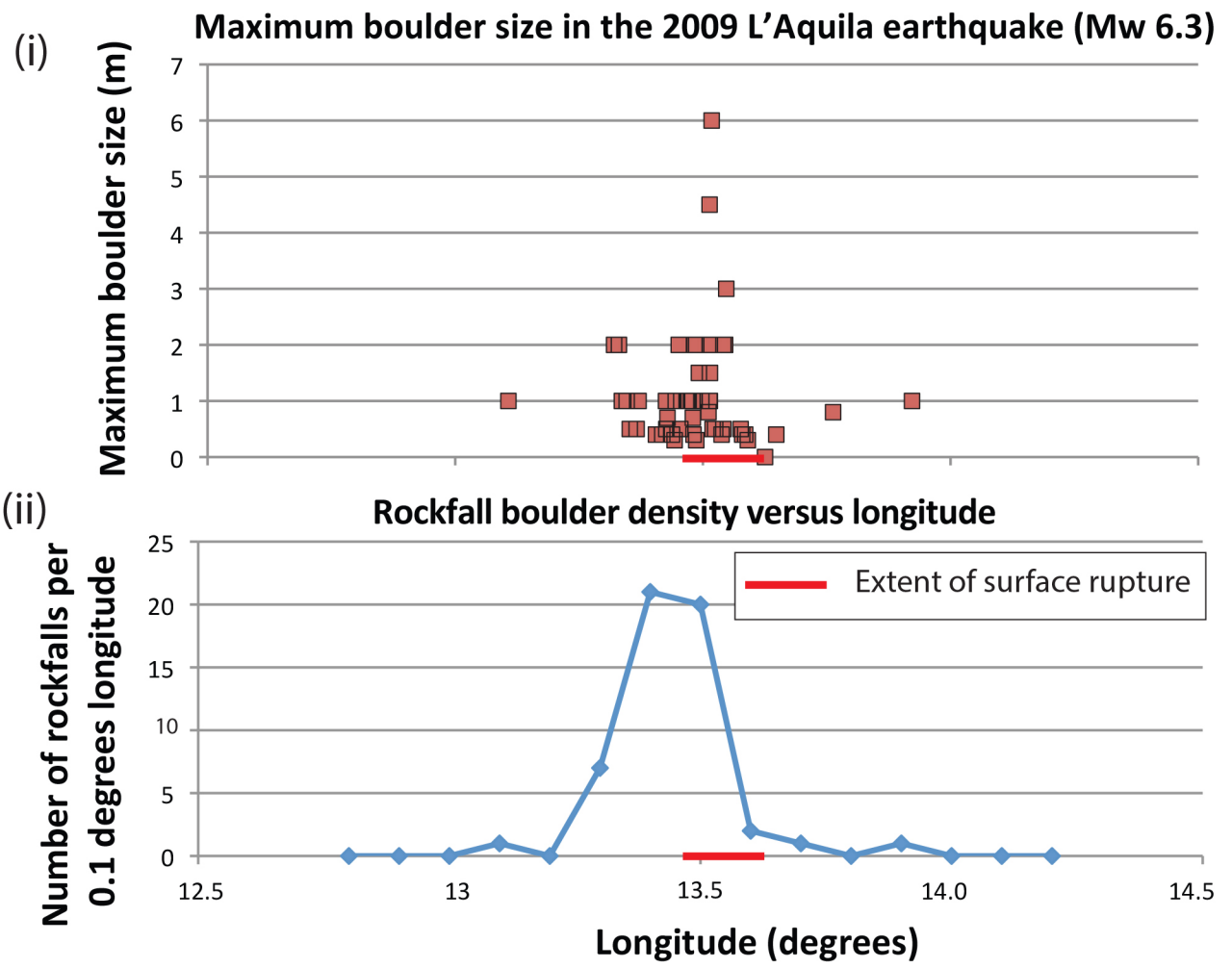

c) Martian dataset - Cerberus Fossae, Roberts et al. (2012)

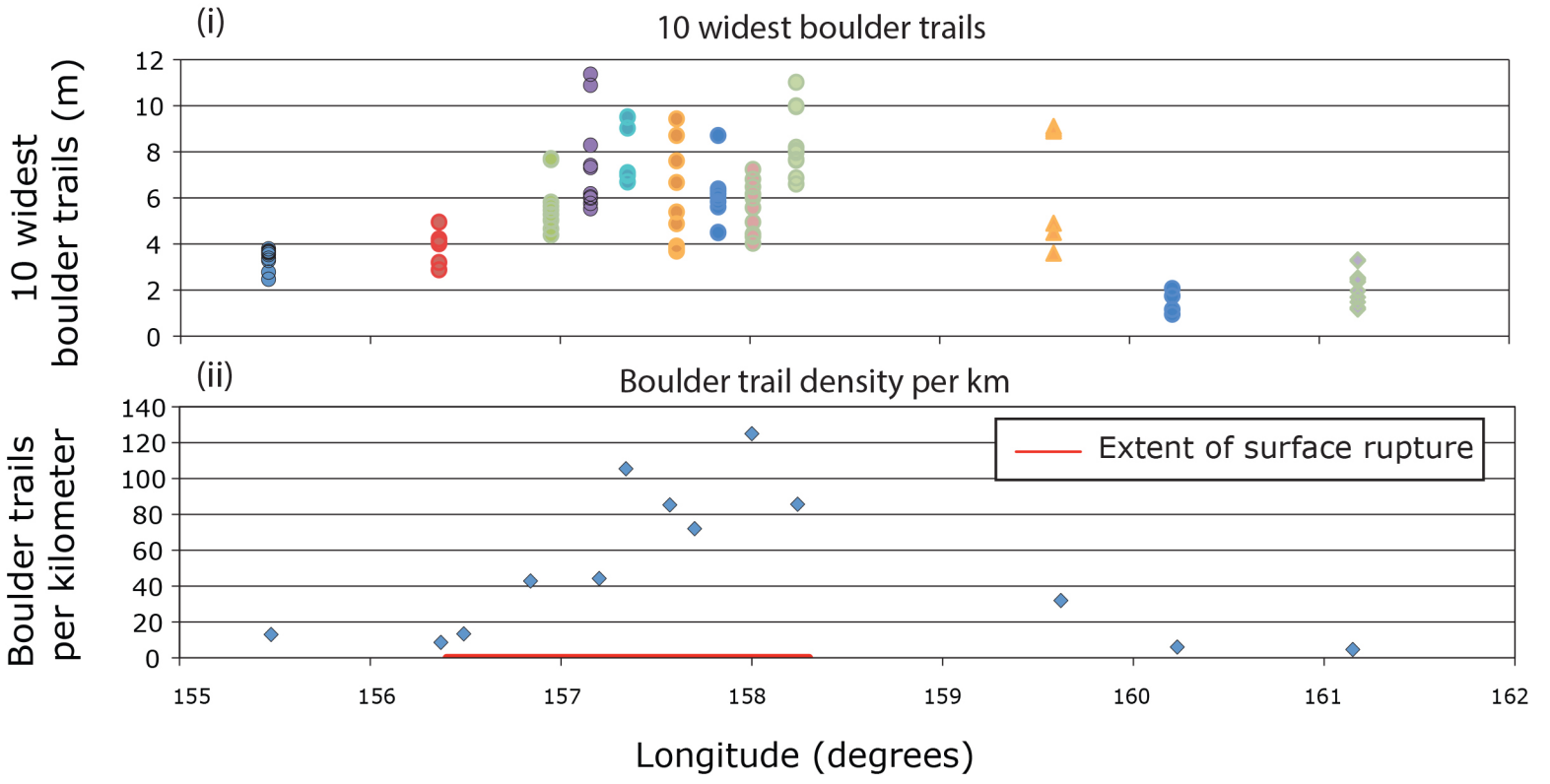

Figure 2

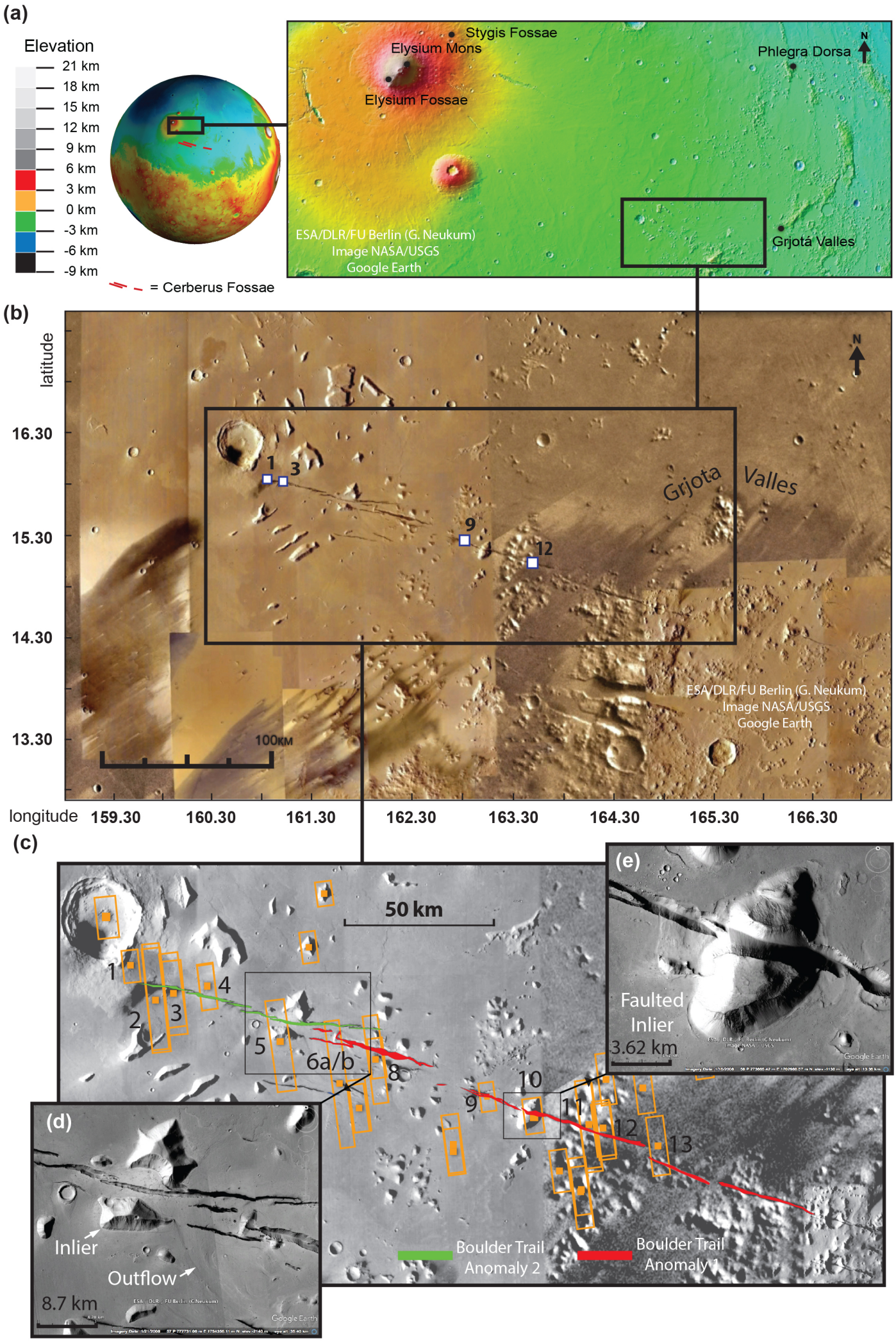
(a)
Elevation
21 km
18 km
15 km
12 km
9 km
6 km
3 km
0 km
-3 km
-6 km
-9 km
= Cerberus Fossae
Stygis Fossae
Elysium Mons
Elysium Fossae
Phlegra Dorsa
N
ESA/DLR/FU Berlin (G. Neukum)
Image NASA/USGS
Google Earth
Grjotá Valles
(b)
latitude
16.30
15.30
14.30
13.30
longitude
159.30
160.30
161.30
162.30
163.30
164.30
165.30
166.30
1
3
9
12
Grjota Valles
100KM
(c)
50 km
1
2
3
4
5
6a/b
8
9
10
11
12
13
Boulder Trail Anomaly 2
Boulder Trail Anomaly 1
(d)
Inlier
Outflow
8.7 km
(e)
Faulted Inlier
3.62 km

Figure 3

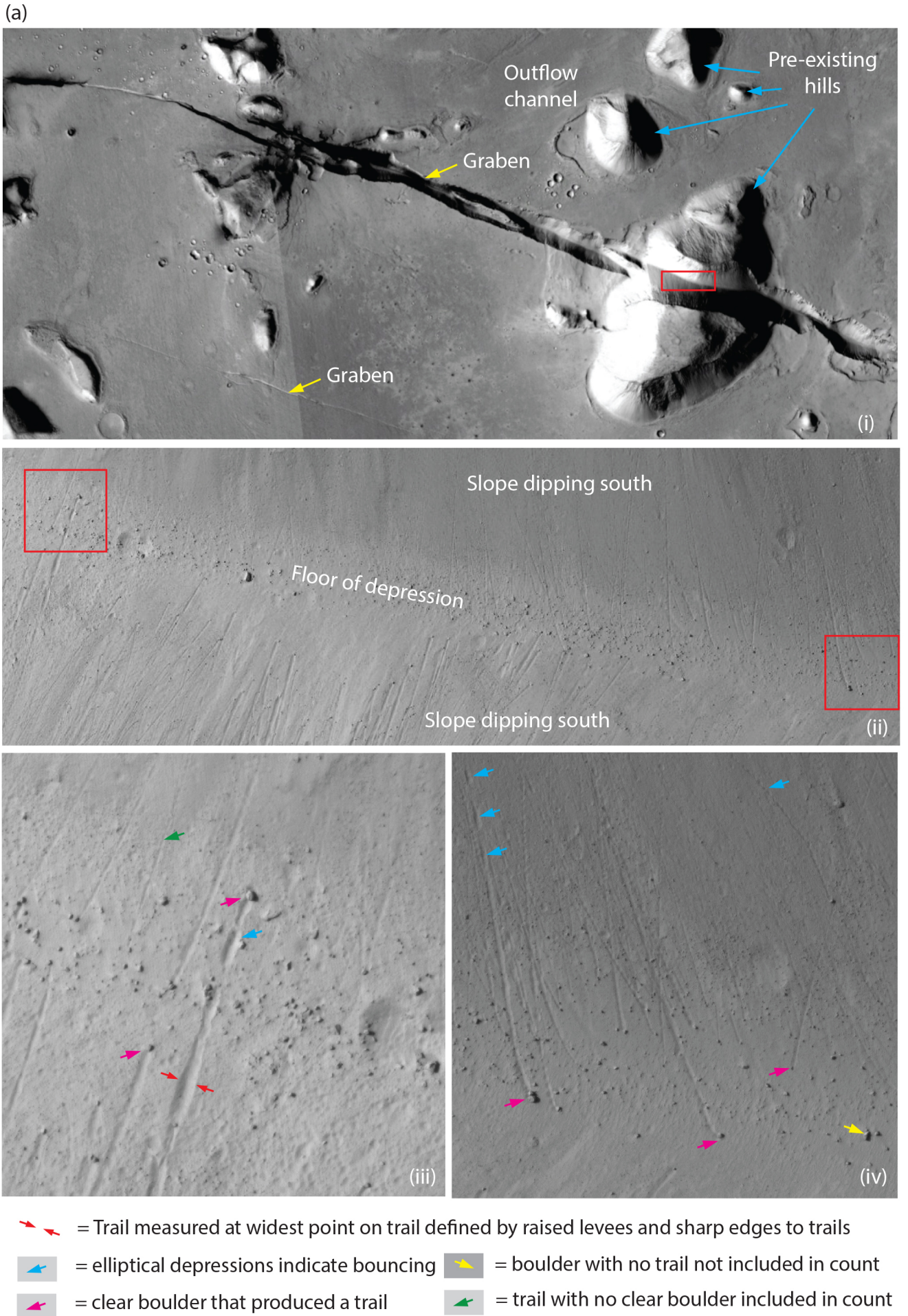
(a)
Outflow channel
Pre-existing hills
Graben
Graben
(i)
Slope dipping south
Floor of depression
Slope dipping south
(ii)
(iii)
(iv)
= Trail measured at widest point on trail defined by raised levees and sharp edges to trails
= elliptical depressions indicate bouncing
= clear boulder that produced a trail
= boulder with no trail not included in count
= trail with no clear boulder included in count

Figure 3 b

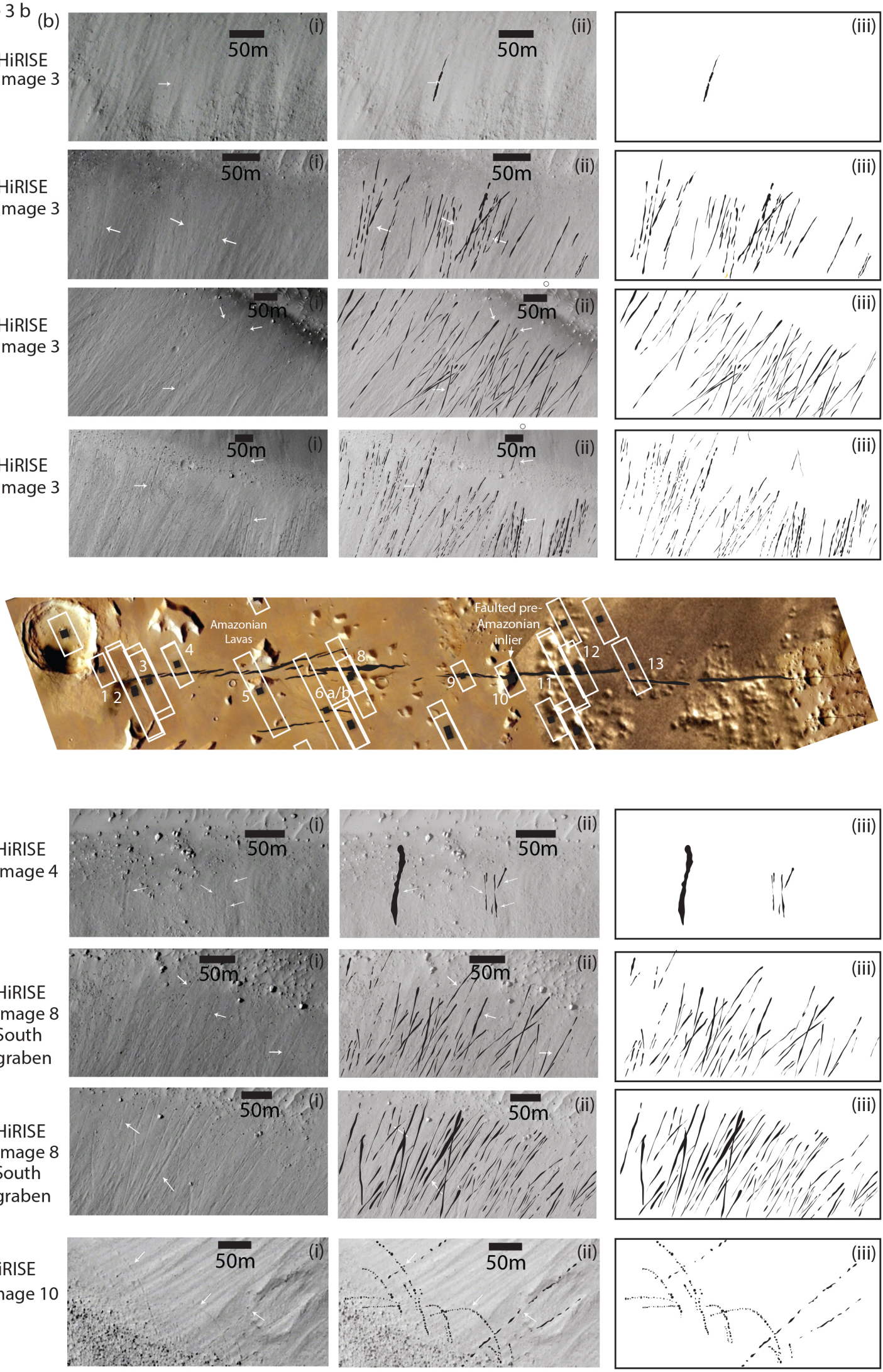
(b)
HiRISE Image 3
HiRISE Image 3
HiRISE Image 3
HiRISE Image 3
(i)
(ii)
(iii)
50m
Amazonian Lavas
Faulted pre-Amazonian inlier
1 2
3
4
5
6a/b
8
9
10
11
12
13
HiRISE Image 4
HiRISE Image 8 South graben
HiRISE Image 8 South graben
HiRISE Image 10

Figure 3 c

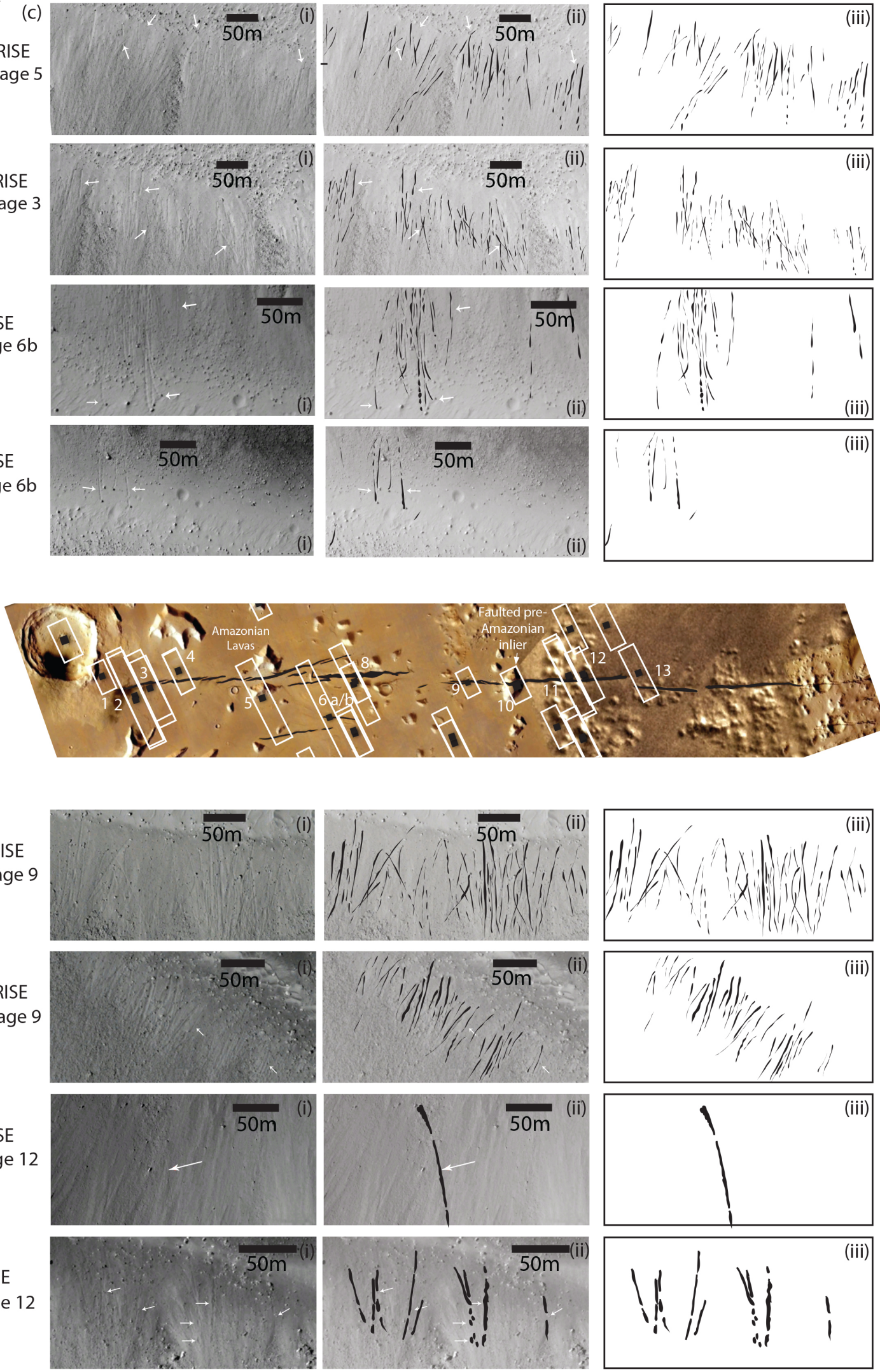
(c)
HiRISE Image 5
HiRISE Image 3
HiRISE Image 6b
HiRISE Image 6b
HiRISE Image 9
HiRISE Image 9
HiRISE Image 12
HiRISE Image 12
50m
(i)
(ii)
(iii)
Amazonian Lavas
Faulted pre-Amazonian inlier
1
2
3
4
5
6a/b
8
9
10
11
12
13

Figure 3 d

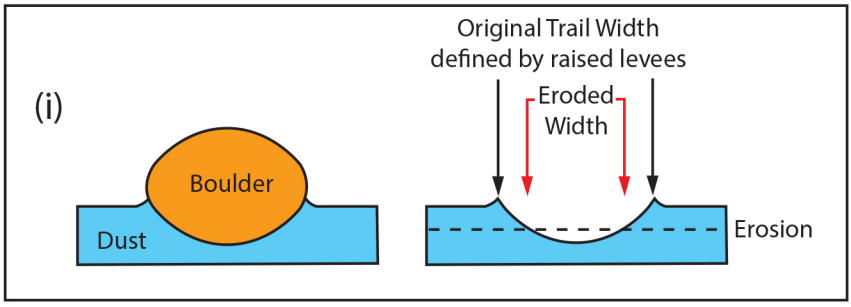

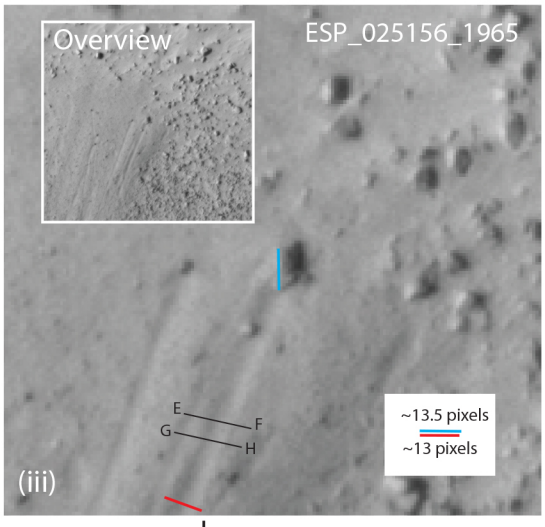

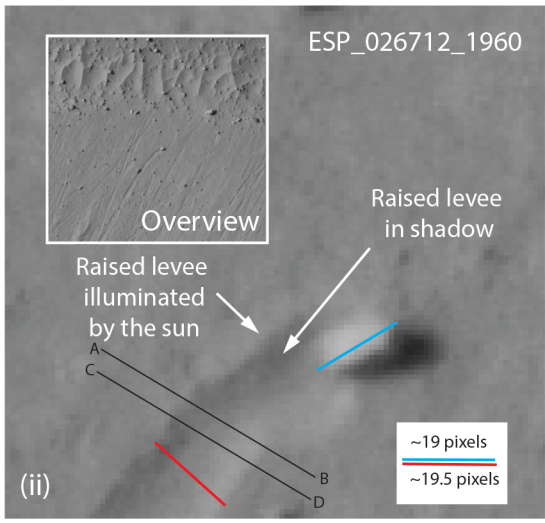

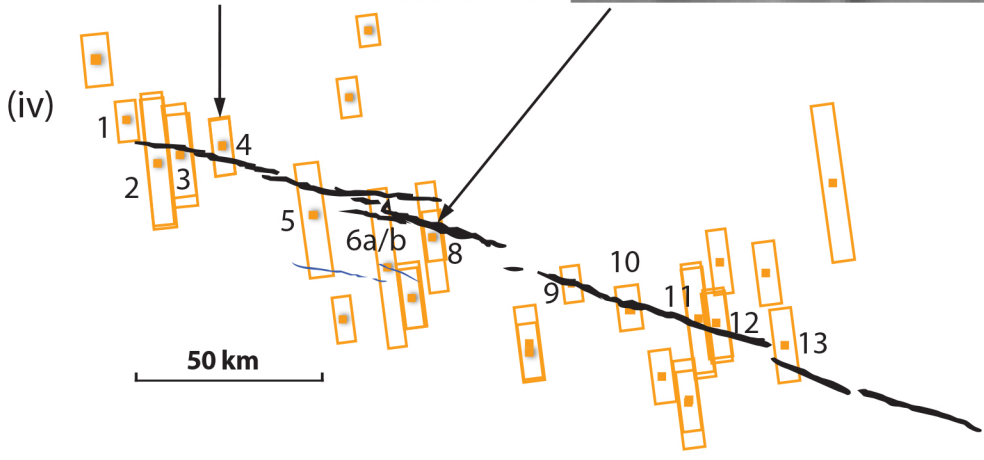

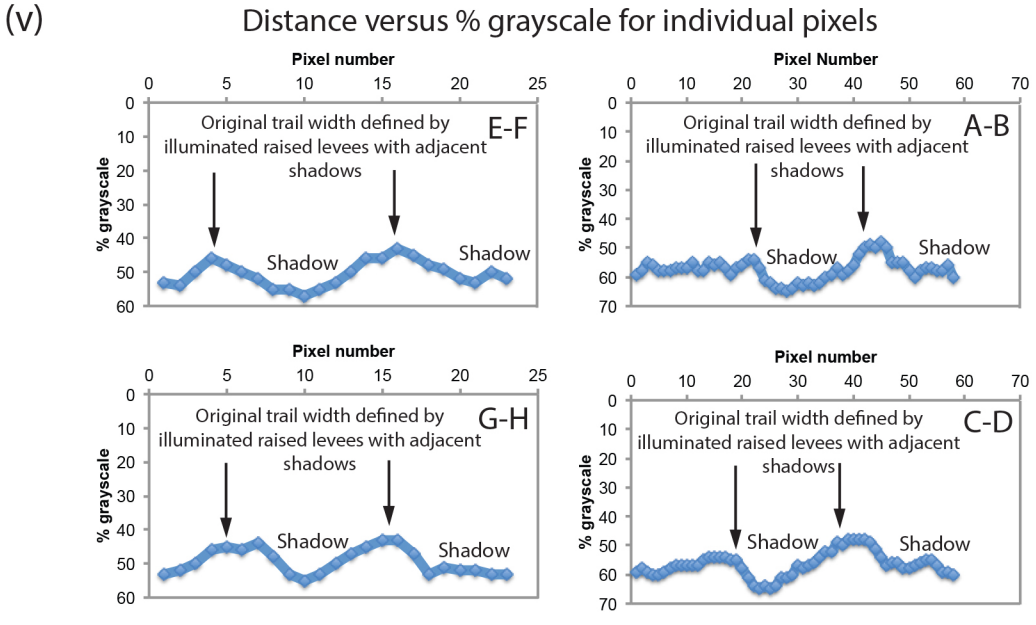

Lower % grayscale values indicate raised, illuminated levees, with higher values indicating shadows produced by the levees

Figure 4 (a)

Image 1.
PSP_008502_1965 HIRISE IMAGE

N

Top right corner of image
16° 10’ 14 • 80” N
160° 35’ 24 • 20” E

Key:

10 Impact craters.

9 Scree slopes, predominatly on the southern side of the depression.

8 Southern cliff/slope (dots denote presence of boulder). Colluvial deposits. Some bedrock lavas exposed?

7 Edge of northern cliff area with dark material forming cliff/slope face (dots denote presence of boulders). Colluvial deposits.

6 Mixed area of material from scree slopes and dunes.

5 Aeolian dunes (Transverse) of North to South orientation. Also, complex aeolian ripple structures (megaripple structures).

4 Lighter coloured areas found only in four locations outside the depression. Possibly terrain (1) that has been cleaned of dust.

3 Line marking the edge of the depression.

2 Smoother, less rugged terrain with aeolian dust deposits

1 Oldest Terrain. Rugged, upstanding ridges. Circular depressions indicate poorly-preserved craters. Cratered lava surface?

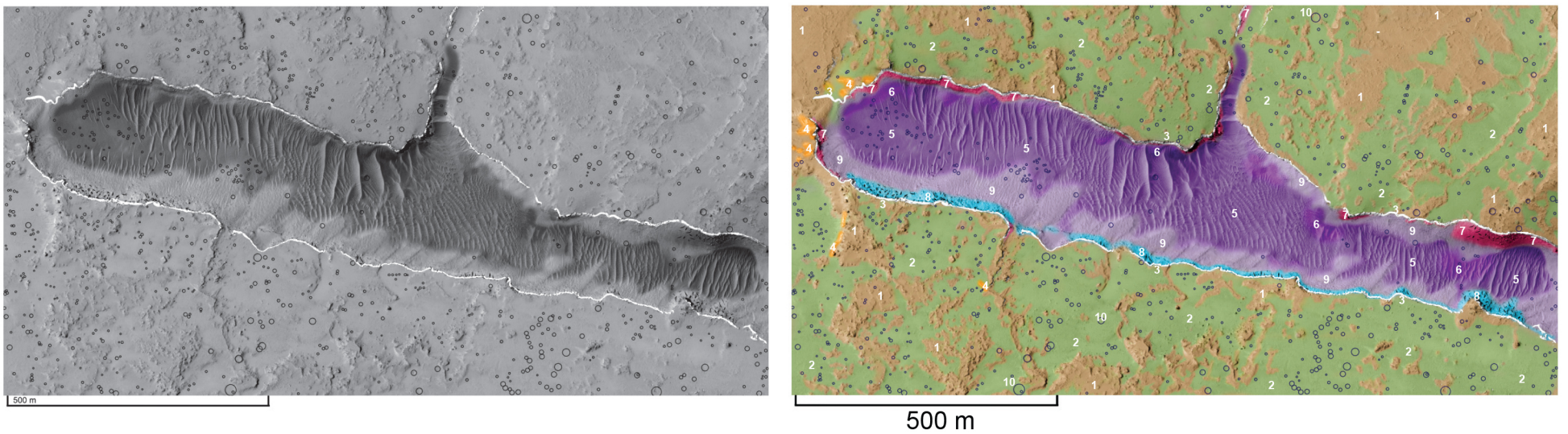

Figure 4 (b)

Image 3.
PSP_006999_1965 HIRISE IMAGE

N

Top right corner of image
16° 9’ 27 • 66” N
160° 52’ 41 • 96” E

Key:

23 Dunes

22 Denotes divide between coaser and finer grained areas.

21 Impact craters.

20 Impact crater with pedestal crater.

19 Inner edge of northern cliff area with dark material forming cliff slope face. The edge appears sharp and lacks boulders / debris.

18 Scree slope on southern side of depression.

17 Area denoting darker material found towards edge of depression (3 locations). May be a lava surface cleared of dust.

16 Defined slope face / cliff face along southern edge of depression, leading to rougher scee slopes down-slope. Some bedrock lava?

15 w / boulders / various sizes of metre-scale.

14 Aeolian dunes (Transverse) of North to South orientation. Also, complex aeolian ripple structures (megaripple structures).

13 Scree slopes, predominatly on the southern side of the depression.

12 Denotes edge of depression area.

11 Possible edge of adjoining depression area.

10 Colluvial deposits. Coarse-grained / darker material.

9 Colluvial deposits. Coarser grained / darker material with evidence of aeolian influence (dune formations).

8 Colluvial deposits, that appear coase-grained.

7 Denotes presence of boulders.

6 Fine grained aeolian dust/sand featuring megaripple structures/trans verse dunes in NE→SW orientation + N→S orientation.

5 Complex dune patterns.

4 Oldest Terrain. Rugged, upstanding ridges. Circular depressions indicate poorly-preserved craters. Possibly a cratered lava surface.

3 Area to lower left of image appeer to display an echelon form. (Also middle left image). Note: presence of aeolian dunes still visible in some higher rigged areas.

2 Mixture of rougher/coaser material, a with more rugged presence of aeolian transvese dunes. Mix of terrains (4), (5) and (6).

1 Outline of more obviously defined terrain (4).

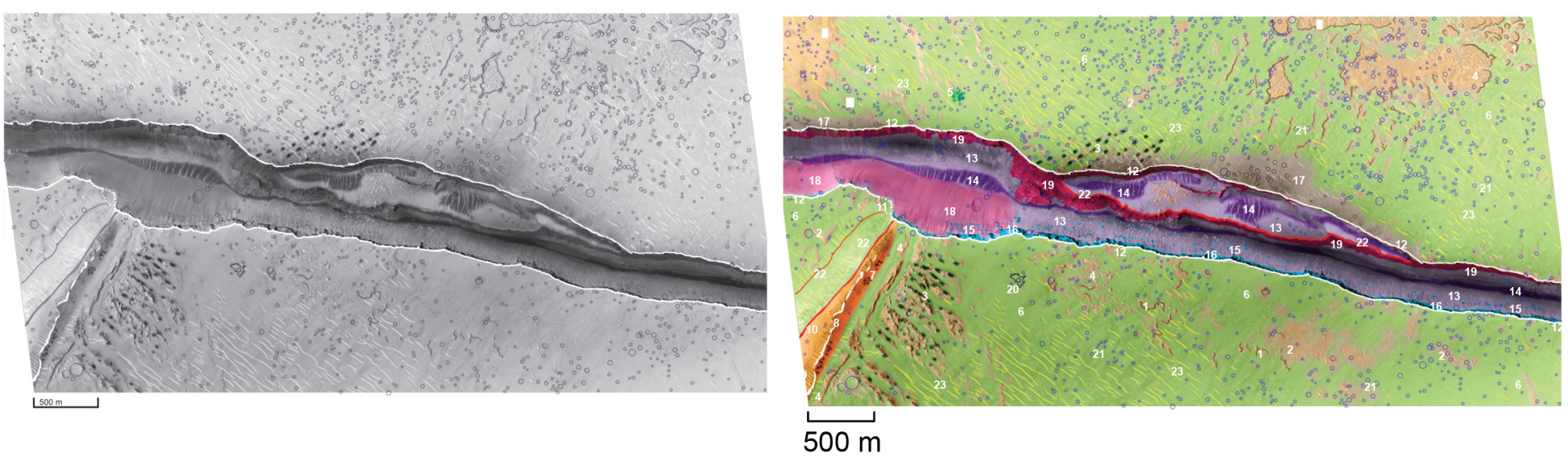

Figure 4 (c)

Image 9.
PSP_006287_1955 HIRISE IMAGE

N

Top right corner of image
15° 32’ 6 • 85” N
162° 44’ 48 • 75” E

Key:

11 Dunes

10 Impact craters.

9 Impact craters with ejecta blankets.

8 Aeolian dunes/ripple structures on floor of depression.

7 Defined slope face/cliff face along parts of both the northern and southern edge of the depression. Bedrock lavas?

6 Colluvial deposits. Inner edge/slope of northern part of depression with dark material forming the cliff slope face.

5 Colluvial deposits. Inner edge/slope of southern part of depression with dark material forming the cliff slope face. Note the presence of fallen boulders from cliff face located towards the base of the depression.

4 Line denotes the edge of the depression.

3 Fine grained aeolian dust/sand pitted with impact craters.

2 Lines denote higher, ridged areas

1 Oldest Terrain. Rugged, up-standing ridges. Possibly a cratered lava surface.

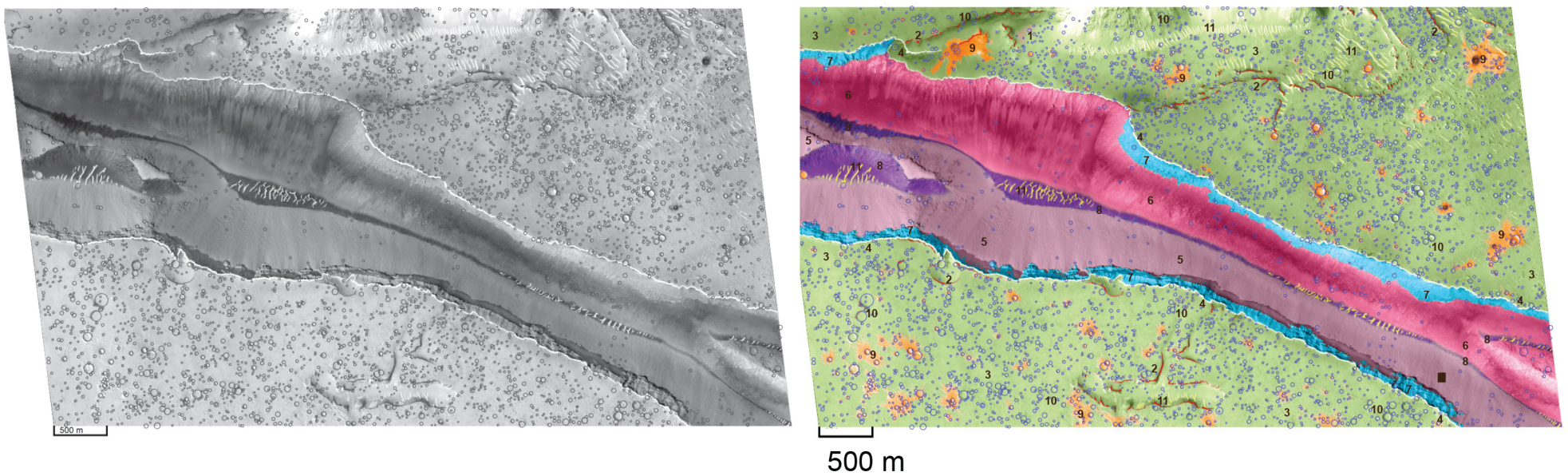

Figure 4 (d)

Image 12.
PSP_010361_1955 HIRISE IMAGE

N

Top right corner of image
15° 21’ 3 • 11” N
163° 25’ 47 • 94” E

Key:

17 Unidentified Structure – Possible impact crater or ridge/upland area.

16 Aeolian Dunes – Present both in and out of the depression. These Aeolian dunes found in the depression form megaripple structures.

15 Impact craters with significant degredation, with some detail lacking, with eroded rims, eroded interiors, in-filled interiors.

14 Impact craters with ejecta blankets.

13 Impact craters.

12 Colluvial deposits.

11 Colluvial deposits lower on slope.

10 Inner edge/slope of depression, forming smooth and even scree slope.

9 A mix of terrain (7 and 10).

8 Defined slope face/cliff face along parts of both the north and south edge of the depression. Exposed bedrock (lavas?) with colluvial deposits lower on the slopes. Towards the east of the image, the defined slope face/cliff face descends down to the depression floor. Colluvium covered in boulders in places.

7 Colluvial deposits. Inner edge/slope of southern part of depression with dark material forming the cliff slope face – Note presence of fallen boulders from cliff face located towards foot of depression.

6 Aeolian dunes/ripple structures on floor of depression.

5 Denotes Edge of Depression.

4 Divide – Between two similar areas (fine grained aeolian areas). The line is demarked by presence of small boulders and a small difference in elevation between the two areas. Generally, the areas to the North and East of the line appear to be slightly lower in elevation, with the line marking a minor minor scree slope. Relative age of material either side of the divide difficult to discern. Dunes/impact craters are similar on both sides.

3 Fine Grained Aeolian dust/sand. Megaripple structures, impact craters and buried craters.

2 Fine Grained Aeolian Area of Lower Elevation than terrain (3). Similar to (7), but with a indistinct hummocky appearance. Predominates in southern region of image.

1 Oldest Terrain. Rugged, high-standing ridges. Possibly a cratered lava surface.

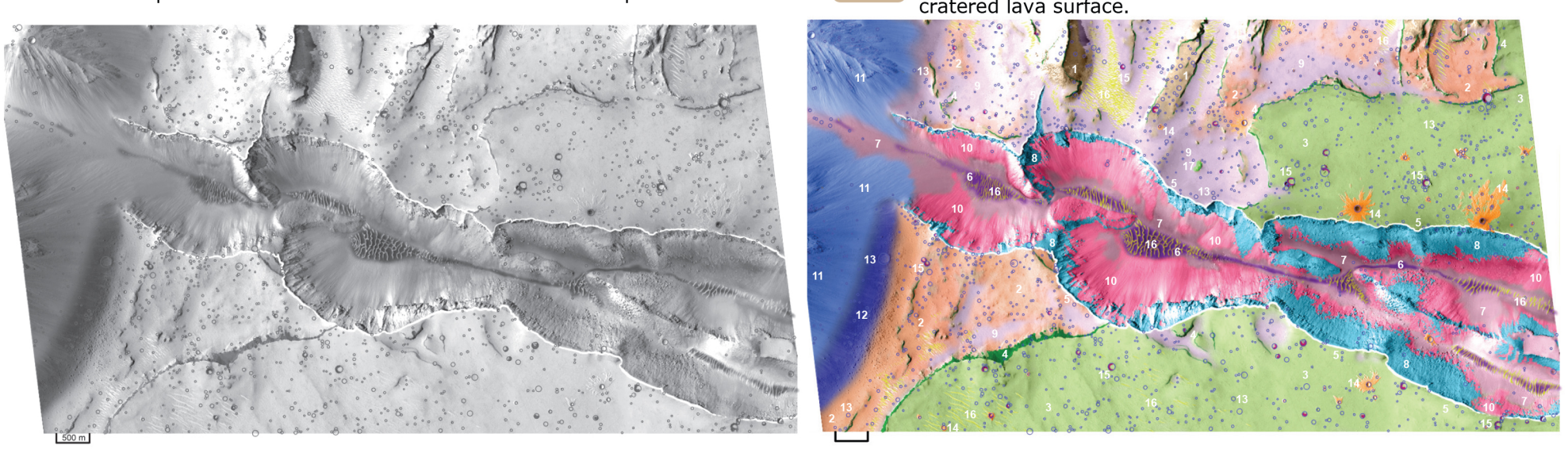

Figure 5

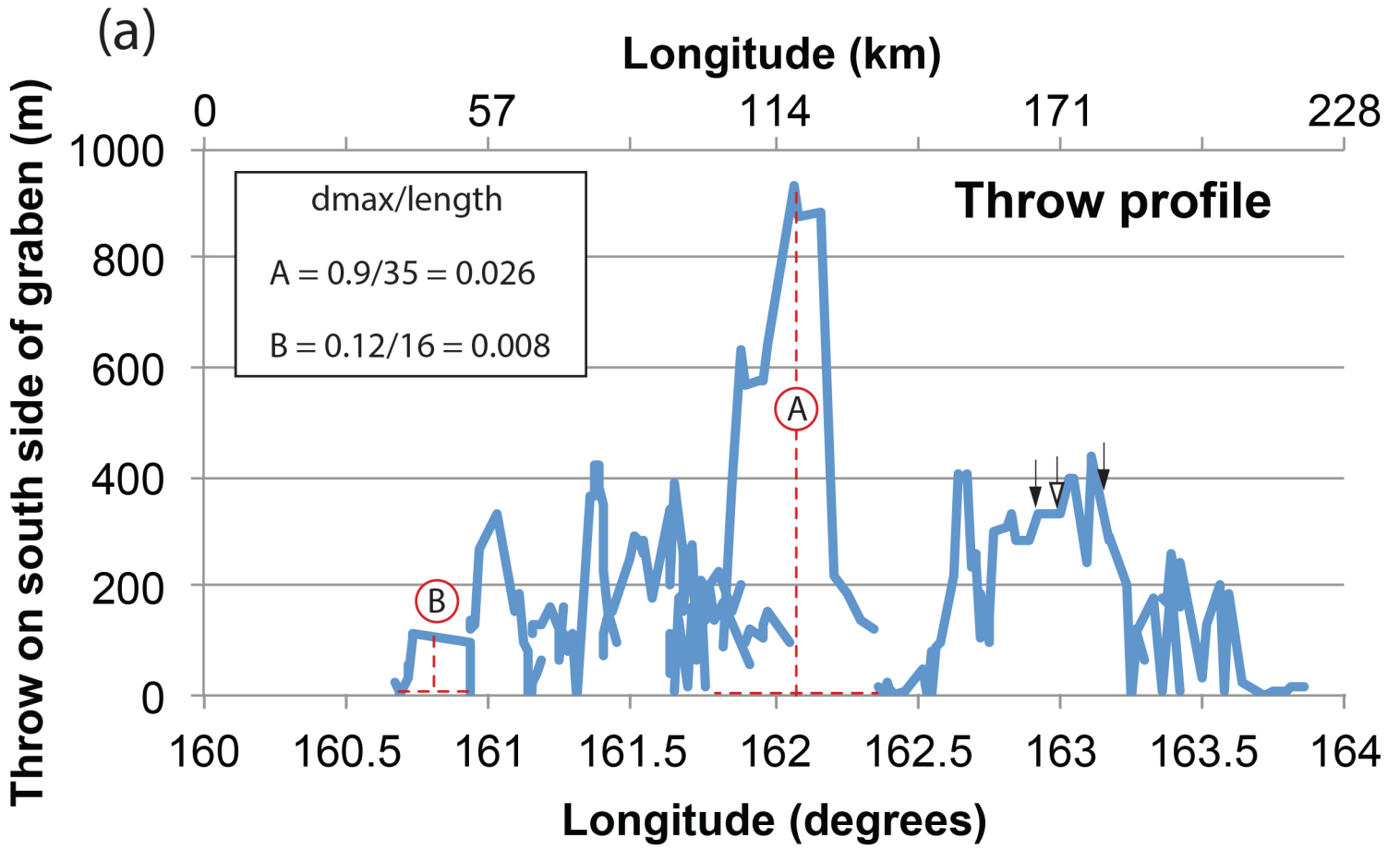
(a)
Longitude (km)
0
57
114
171
228
Throw on south side of graben (m)
1000
800
600
400
200
0
dmax/length
A = 0.9/35 = 0.026
B = 0.12/16 = 0.008
Throw profile
A
B
160
160.5
161
161.5
162
162.5
163
163.5
164
Longitude (degrees)

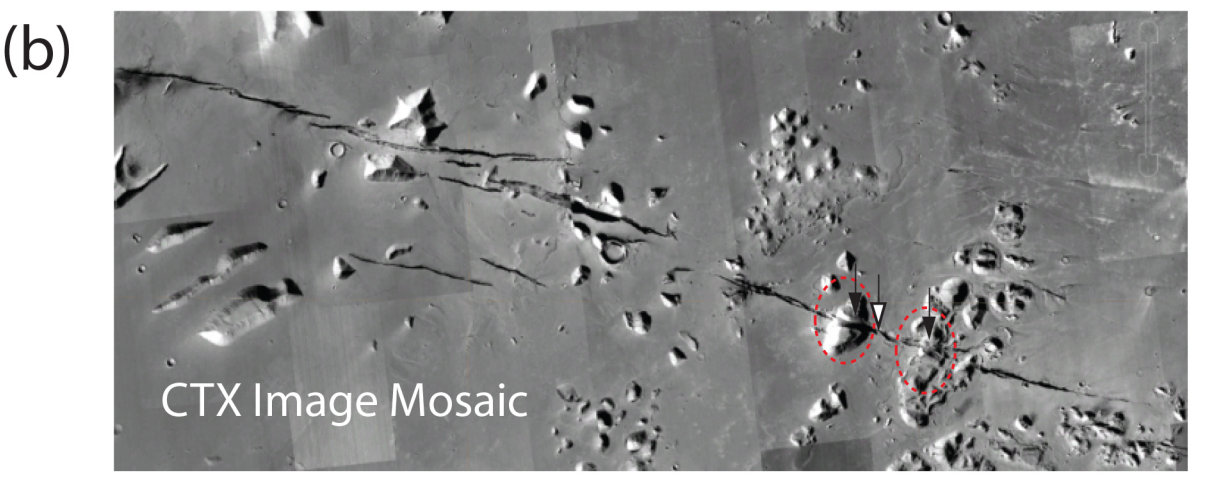
(b)
CTX Image Mosaic

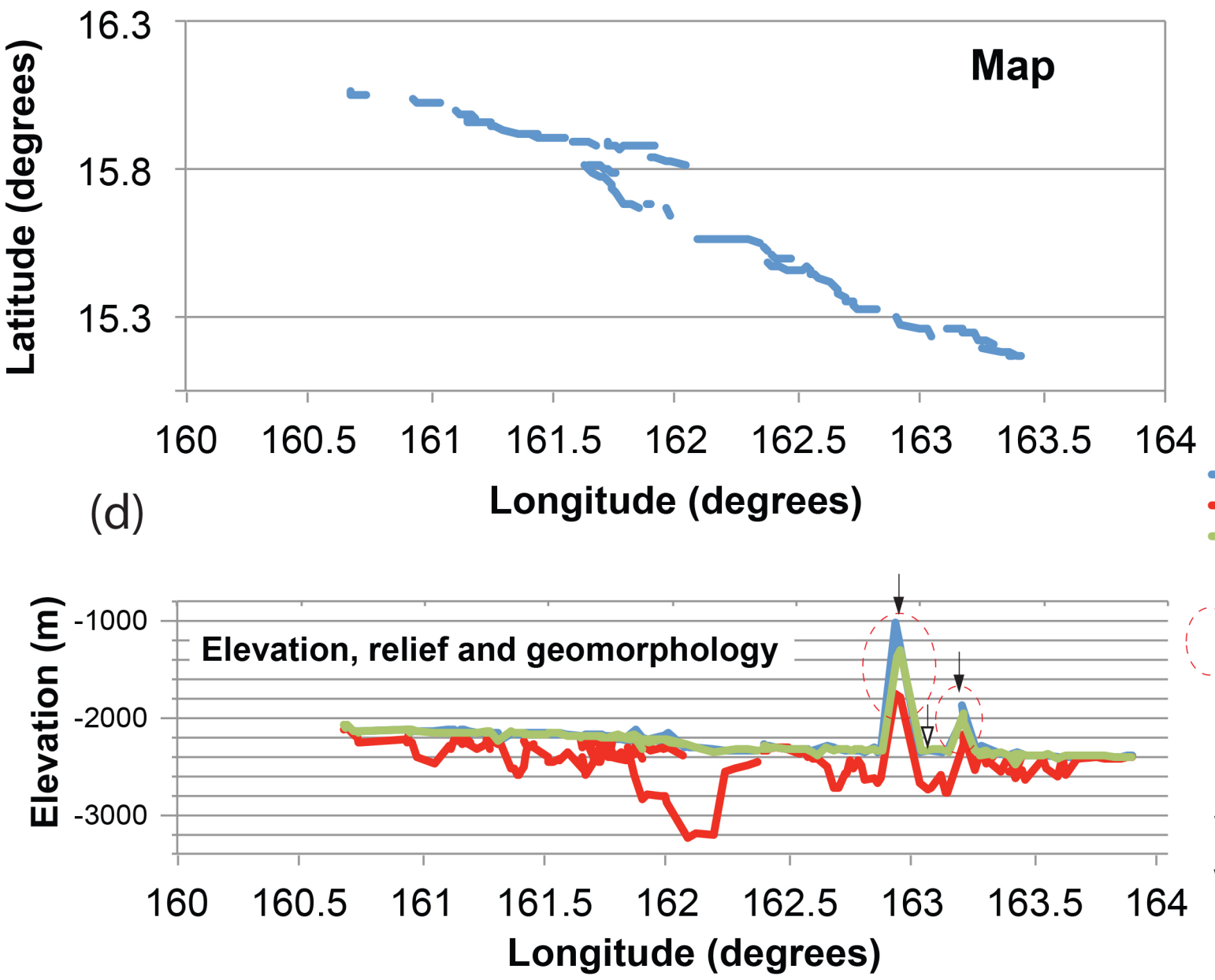
(c)
16.3
15.8
15.3
Latitude (degrees)
Map
160
160.5
161
161.5
162
162.5
163
163.5
164
Longitude (degrees)
(d)
-1000
-2000
-3000
Elevation (m)
Elevation, relief and geomorphology
160
160.5
161
161.5
162
162.5
163
163.5
164
Longitude (degrees)
South
Graben
North
Pre-faulting topography preserved in graben ruling out collapse as the graben forming mechanism
Points with similar vertical throw (see a), showing that the faults offset pre-existing topography

Figure 6

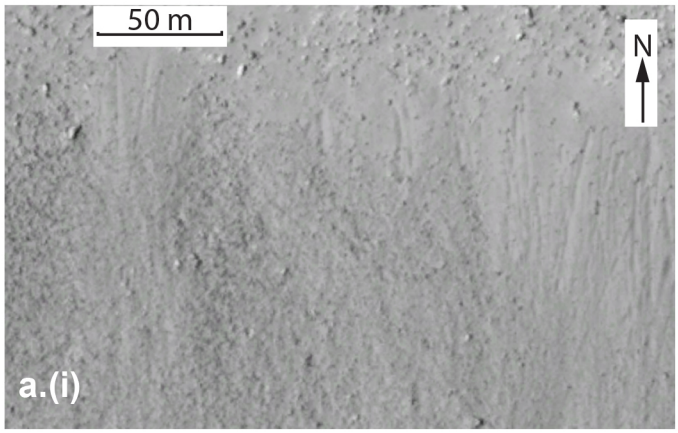
50 m
N
a.(i)

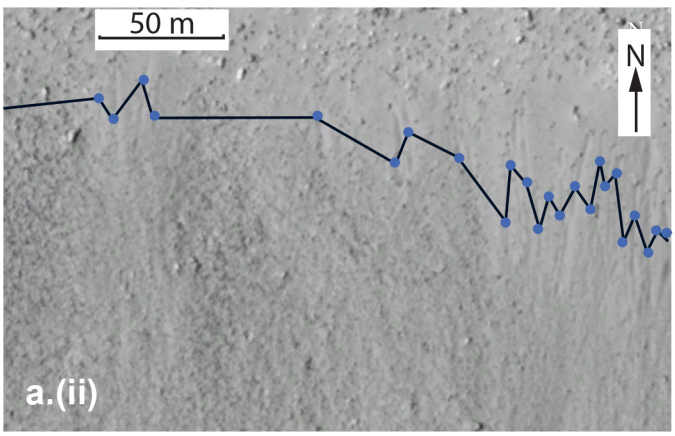
50 m
N
a.(ii)

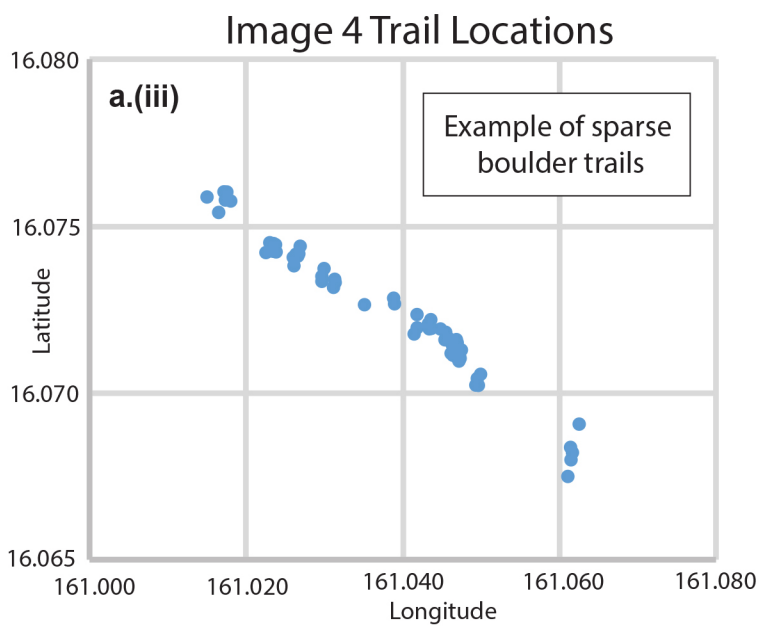
Image 4 Trail Locations
a.(iii)
Example of sparse boulder trails
16.080
16.075
16.070
16.065
Latitude
161.000
161.020
161.040
161.060
161.080
Longitude

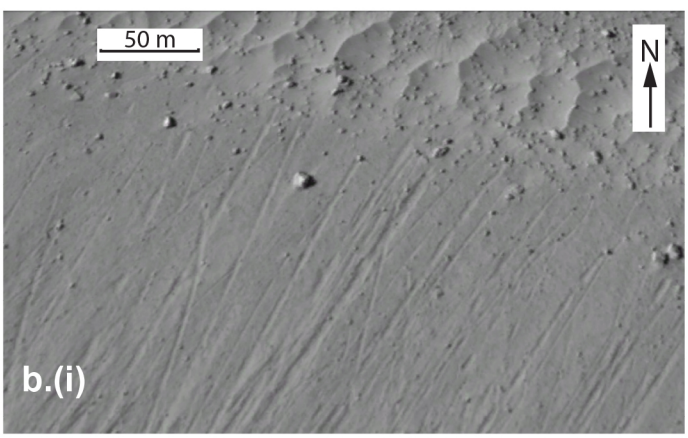
50 m
N
b.(i)

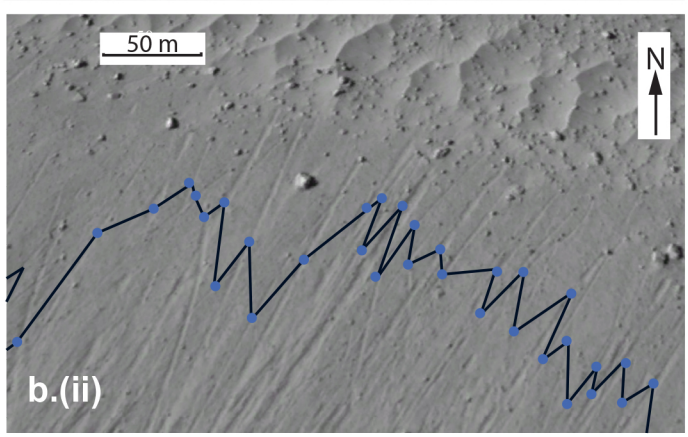
50 m
N
b.(ii)

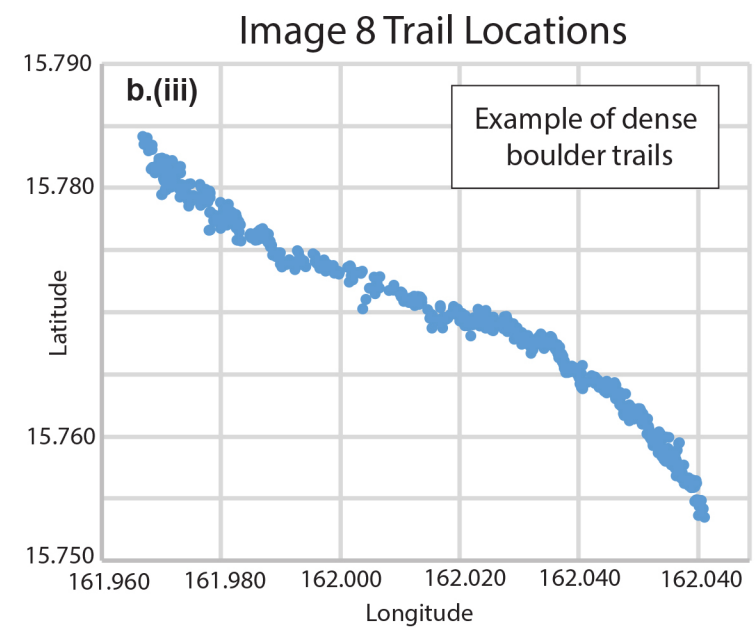
Image 8 Trail Locations
b.(iii)
Example of dense boulder trails
15.790
15.780
15.760
15.750
Latitude
161.960
161.980
162.000
162.020
162.040
162.040
Longitude

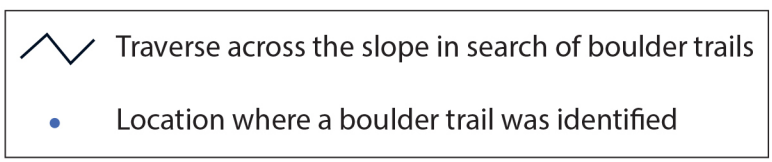
Traverse across the slope in search of boulder trails
Location where a boulder trail was identified

Figure 7

(a) Calibration - 10 Widest Trails

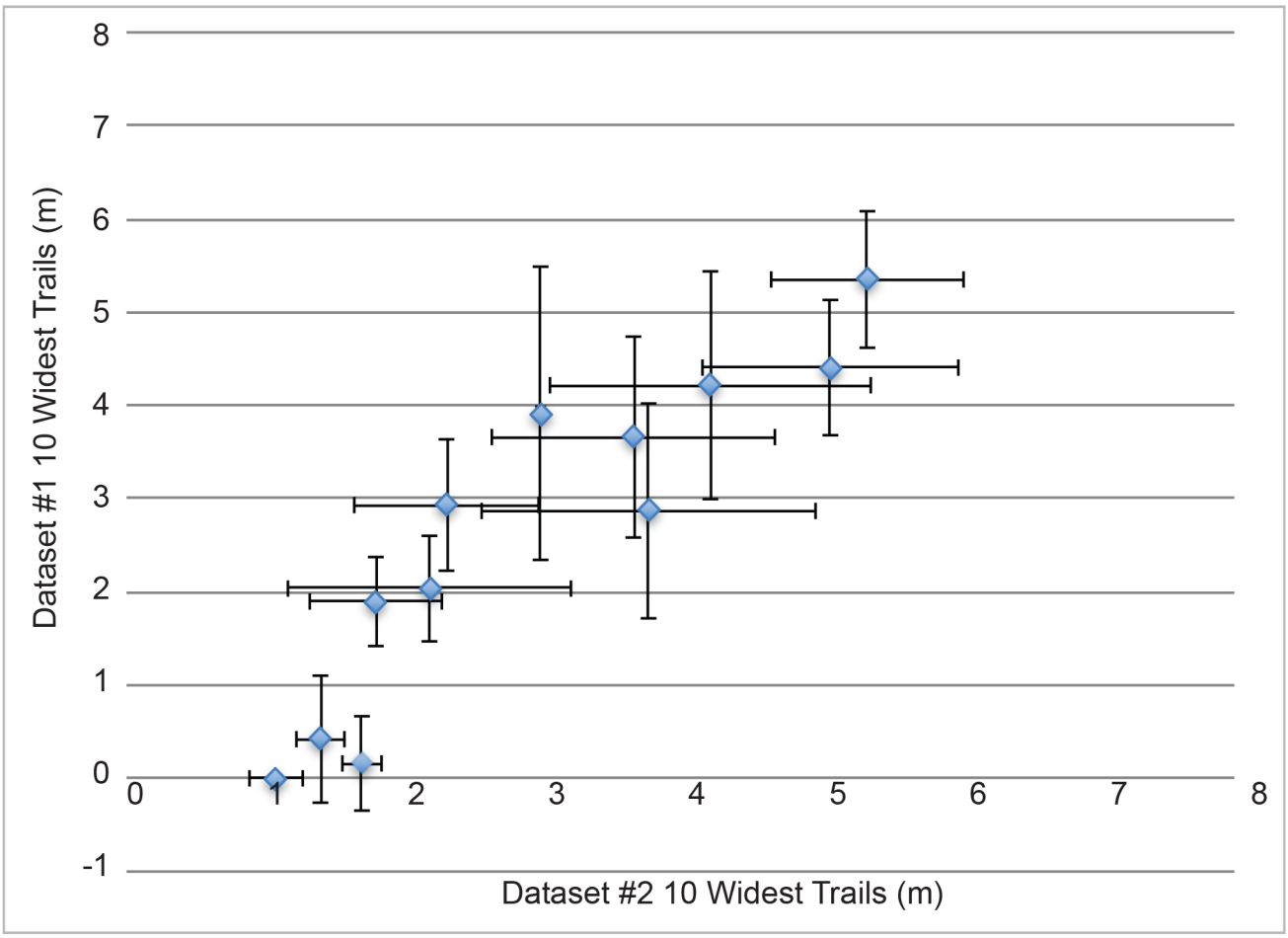

(b) Calibration - Boulder Trail Counts per Kilometre

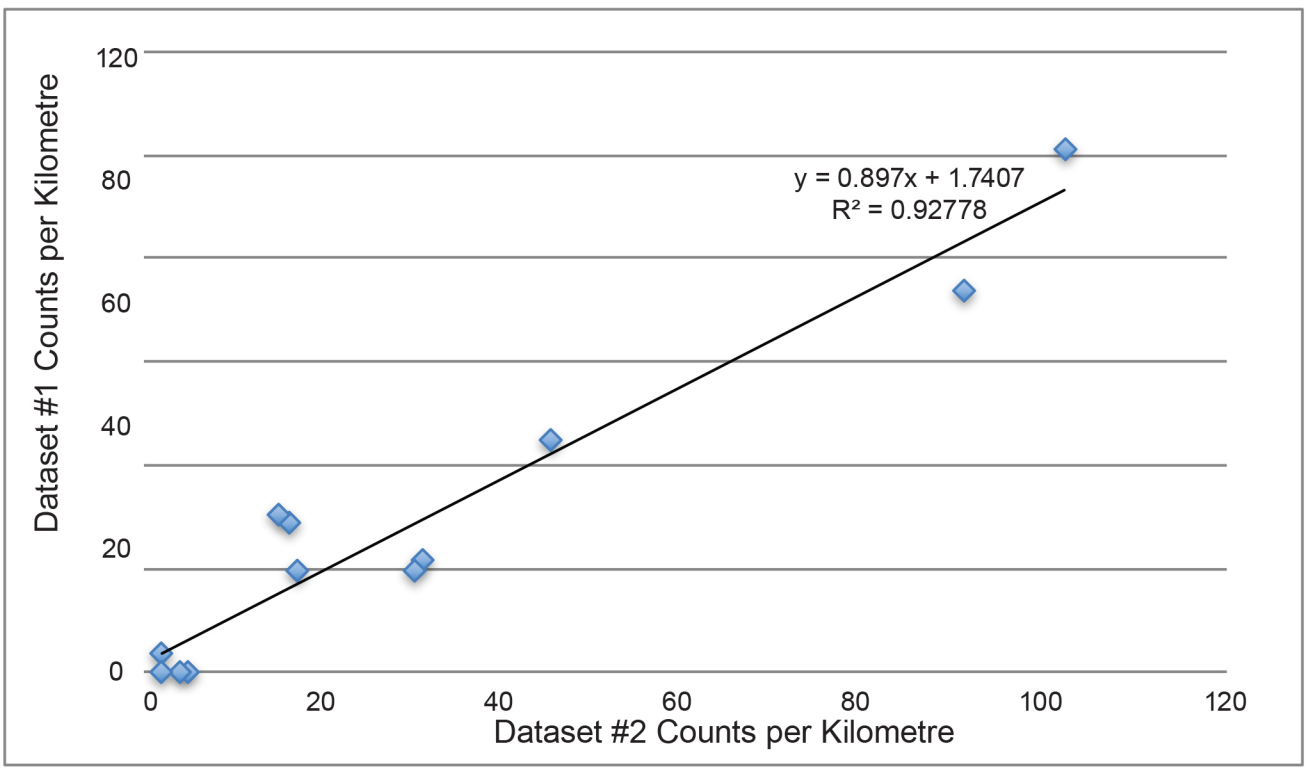

Figure 8

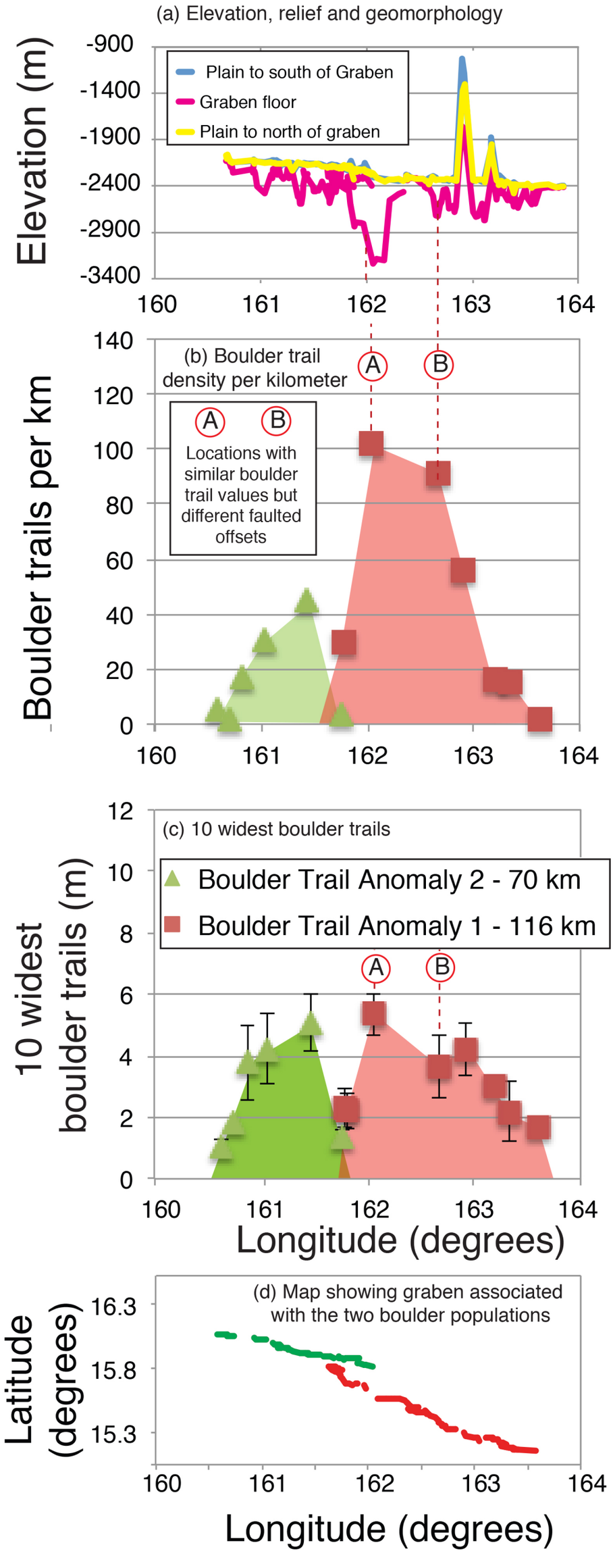
(a) Elevation, relief and geomorphology
Elevation (m)
-900
-1400
-1900
-2400
-2900
-3400
Plain to south of Graben
Graben floor
Plain to north of graben
160
161
162
163
164
(b) Boulder trail density per kilometer
A
B
Locations with similar boulder trail values but different faulted offsets
Boulder trails per km
140
120
100
80
60
40
20
0
(c) 10 widest boulder trails
Boulder Trail Anomaly 2 - 70 km
Boulder Trail Anomaly 1 - 116 km
10 widest boulder trails (m)
12
10
8
6
4
2
0
Longitude (degrees)
(d) Map showing graben associated with the two boulder populations
Latitude (degrees)
16.3
15.8
15.3
Longitude (degrees)

Figure 9

(a) Maps showing the relatively continuous fault length of Cerberus Fossae compared to Grjota Valles and the extent of boulder trail anomalies (Bta).

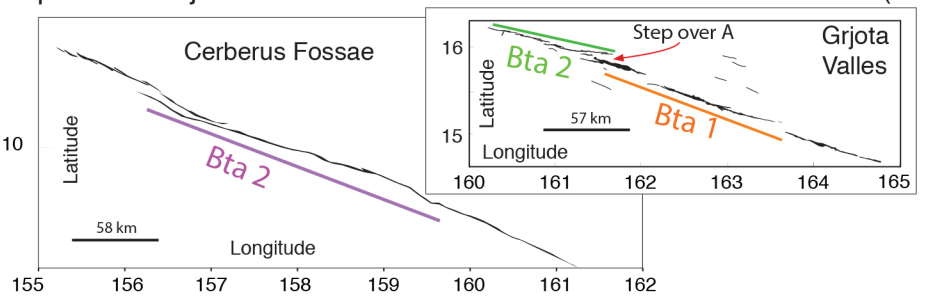

(b) Boulder trail density per kilometre

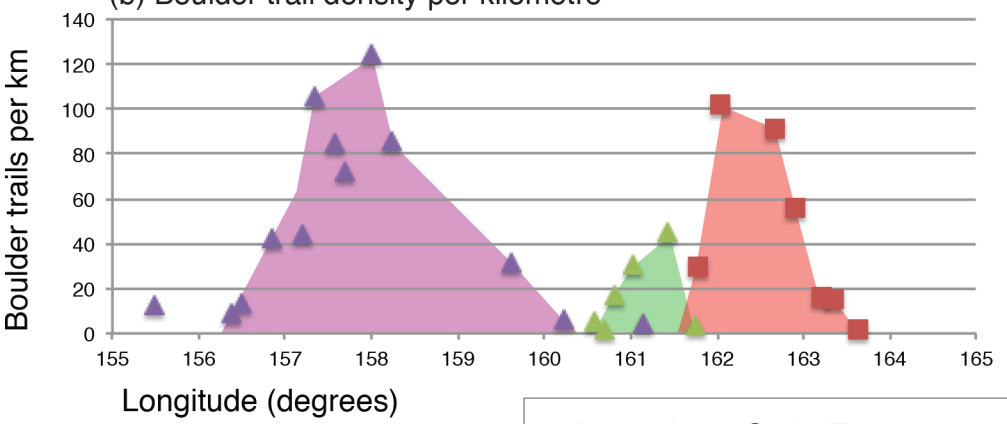

(c) 10 widest boulder trails

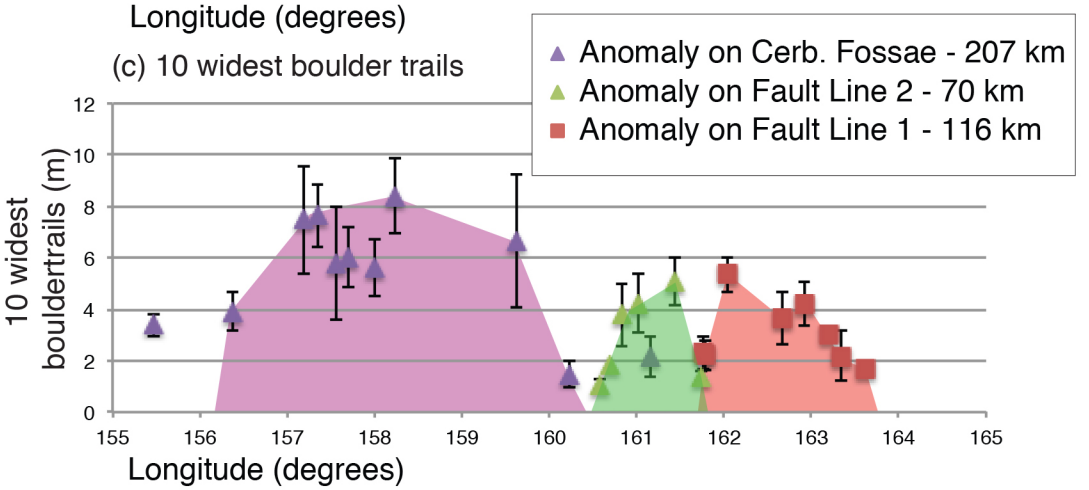

(d) Speculative inference of marsquake magnitude from rupture length

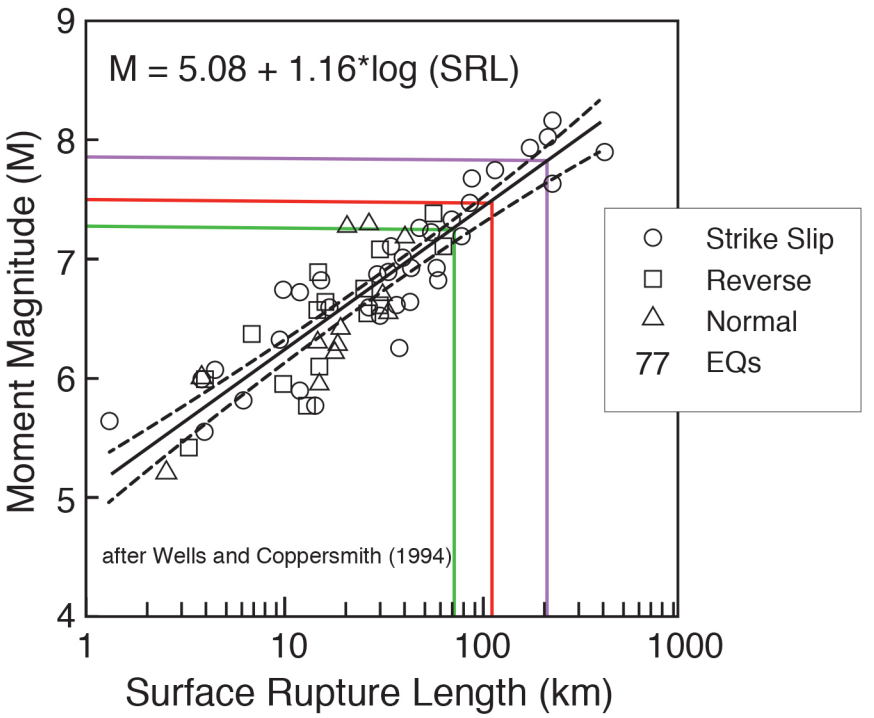

Figure 10

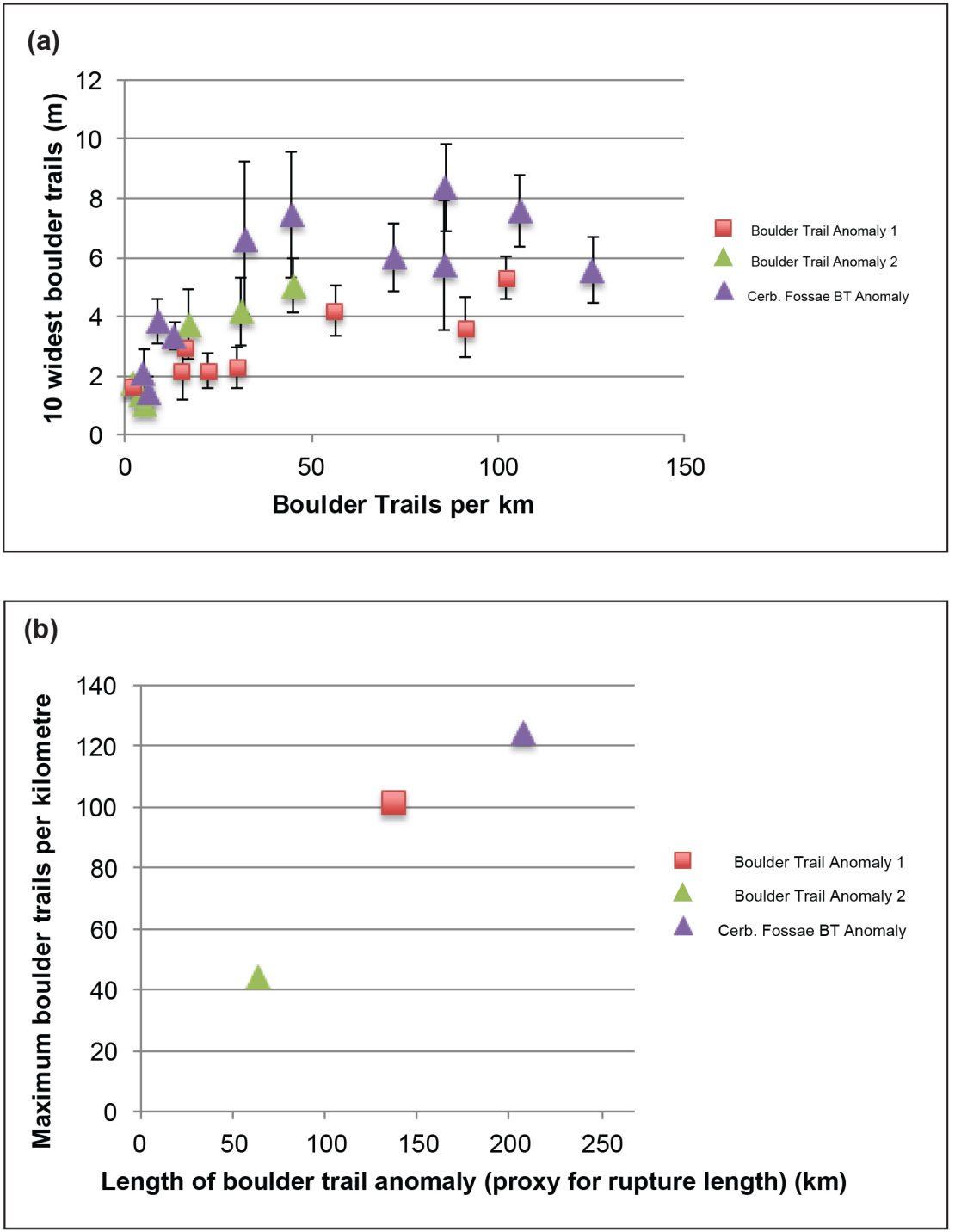
(a)
10 widest boulder trails (m)
0
2
4
6
8
10
12
0
50
100
150
Boulder Trails per km
Boulder Trail Anomaly 1
Boulder Trail Anomaly 2
Cerb. Fossae BT Anomaly
(b)
Maximum boulder trails per kilometre
0
20
40
60
80
100
120
140
0
50
100
150
200
250
Length of boulder trail anomaly (proxy for rupture length) (km)
Boulder Trail Anomaly 1
Boulder Trail Anomaly 2
Cerb. Fossae BT Anomaly

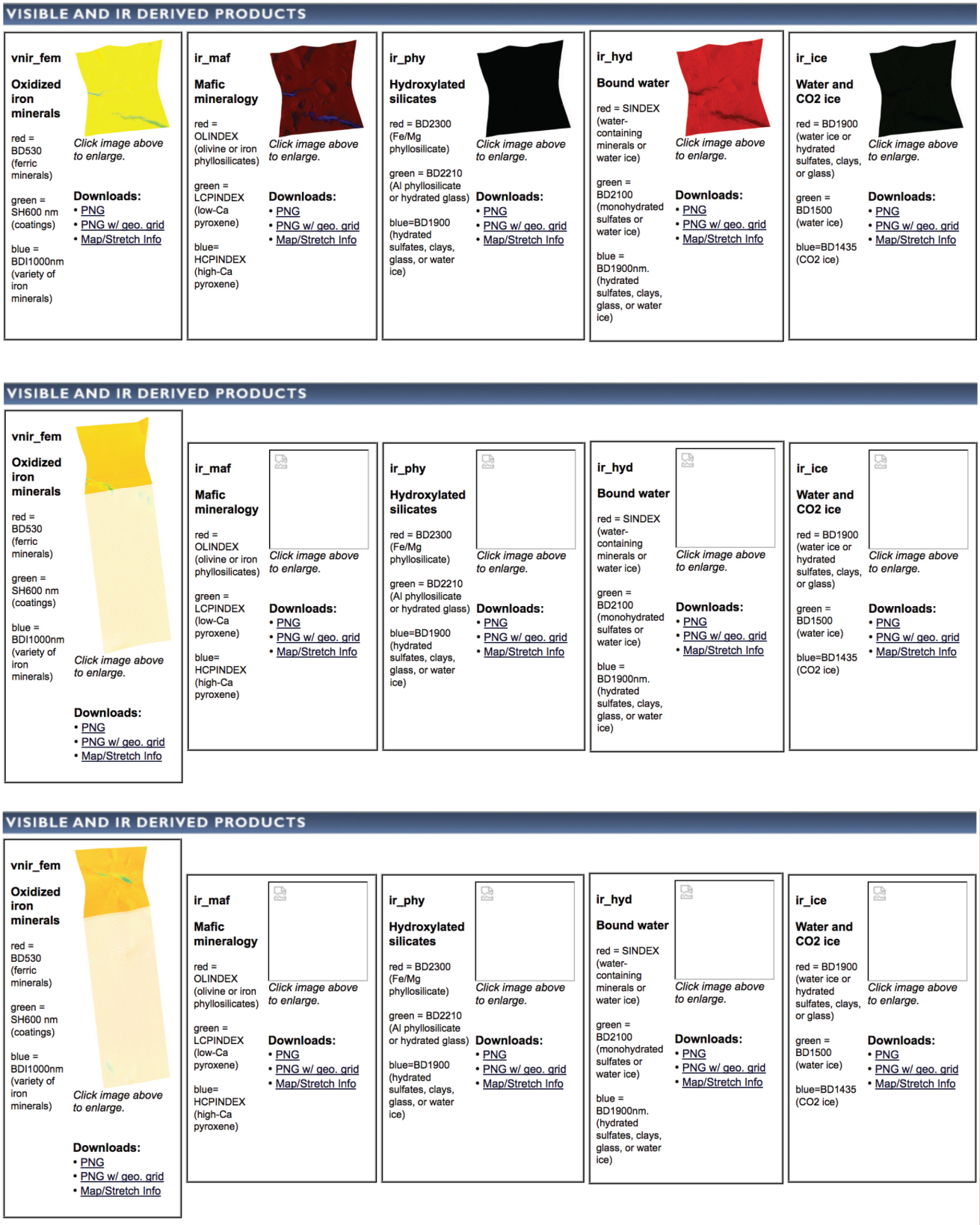

Supplementary Figure S1: Relates to the second point for discussion in the Discussion section of our paper, *2) The effect of local differences lithology and hence weathering/erosion*. The idea that particular lithologies are prone to more or less erosion and as such may control the number and sizes of boulders released from slopes along the graben. S1 is an image from CRISM (Compact Reconnaissance Imaging Spectrometer for Mars) showing that there was no obvious change in the lithology of rocks forming the graben walls. The missing thumbnails are also missing from the CRISM site.

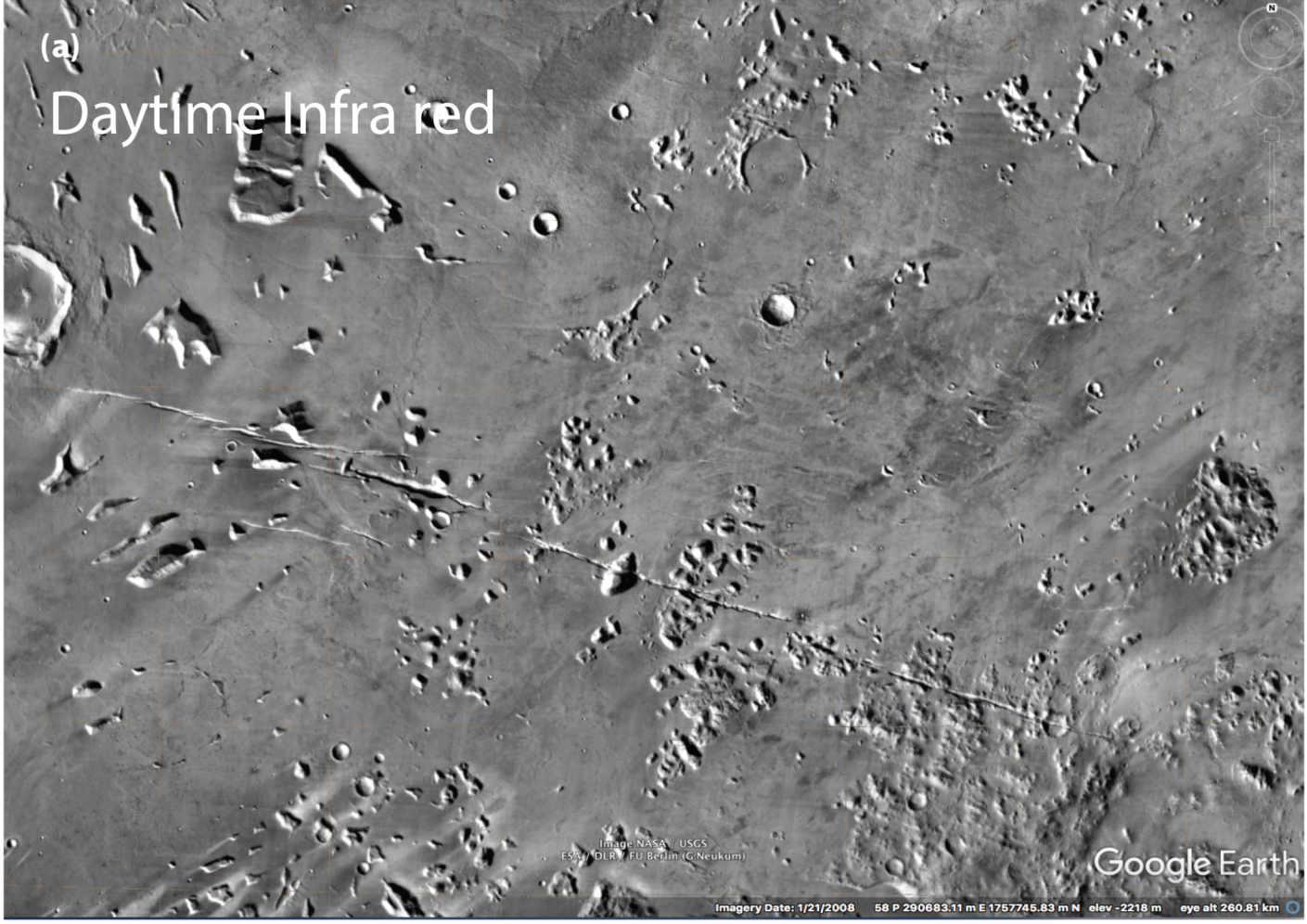

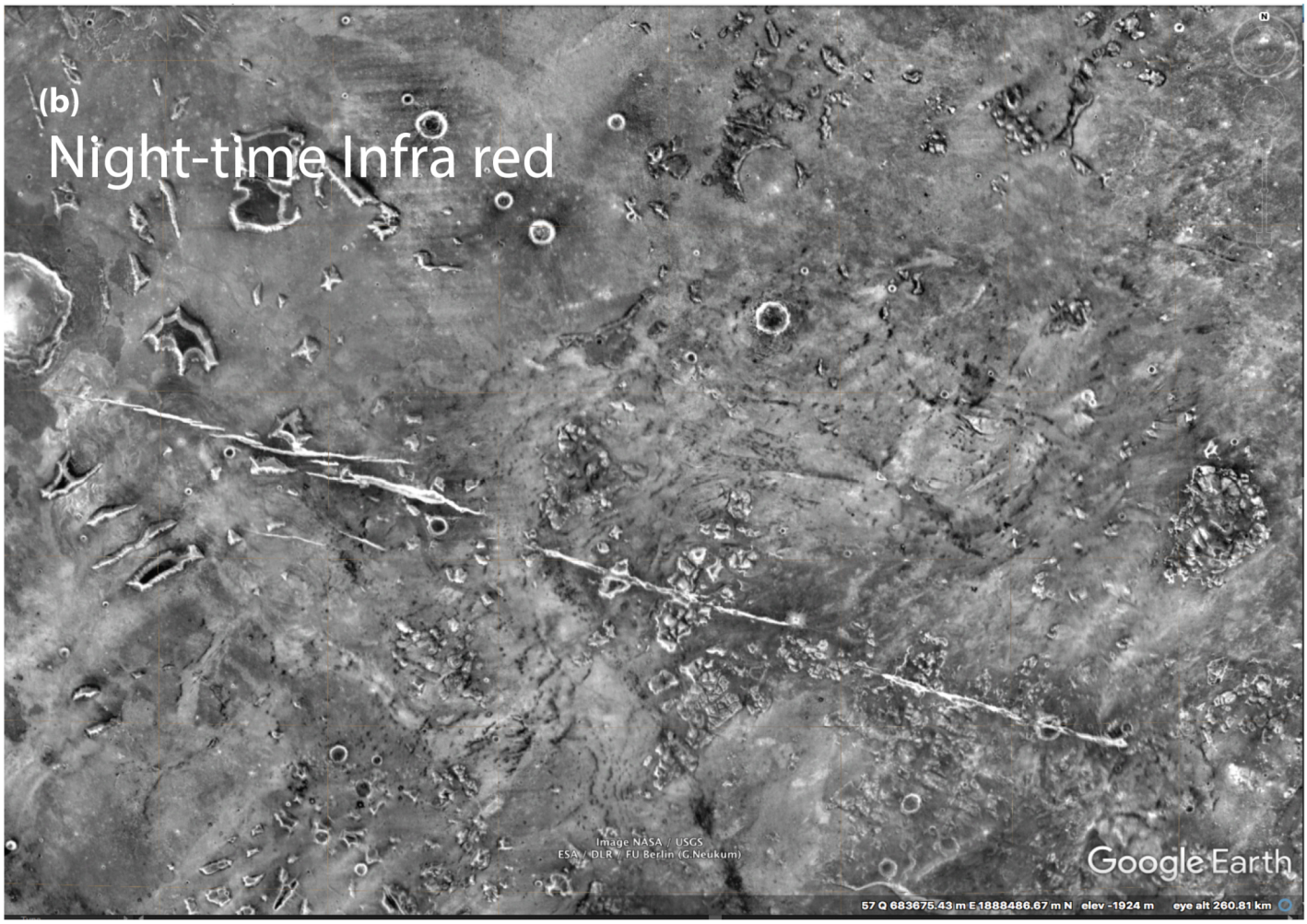

Supplementary Figure S2: Relates to the second point for discussion in the Discussion section of our paper, *2) The effect of local differences lithology and hence weathering/erosion*. The idea that particular lithologies are prone to more or less erosion and as such may control the number and sizes of boulders released from slopes along the graben. S2 a & b are daytime and night-time images from THEMIS (Thermal Emission Imaging System) and shows that there is no obvious change in the lithology of rocks forming the graben walls, highlighting only that the graben walls appear to be formed of bedrock.

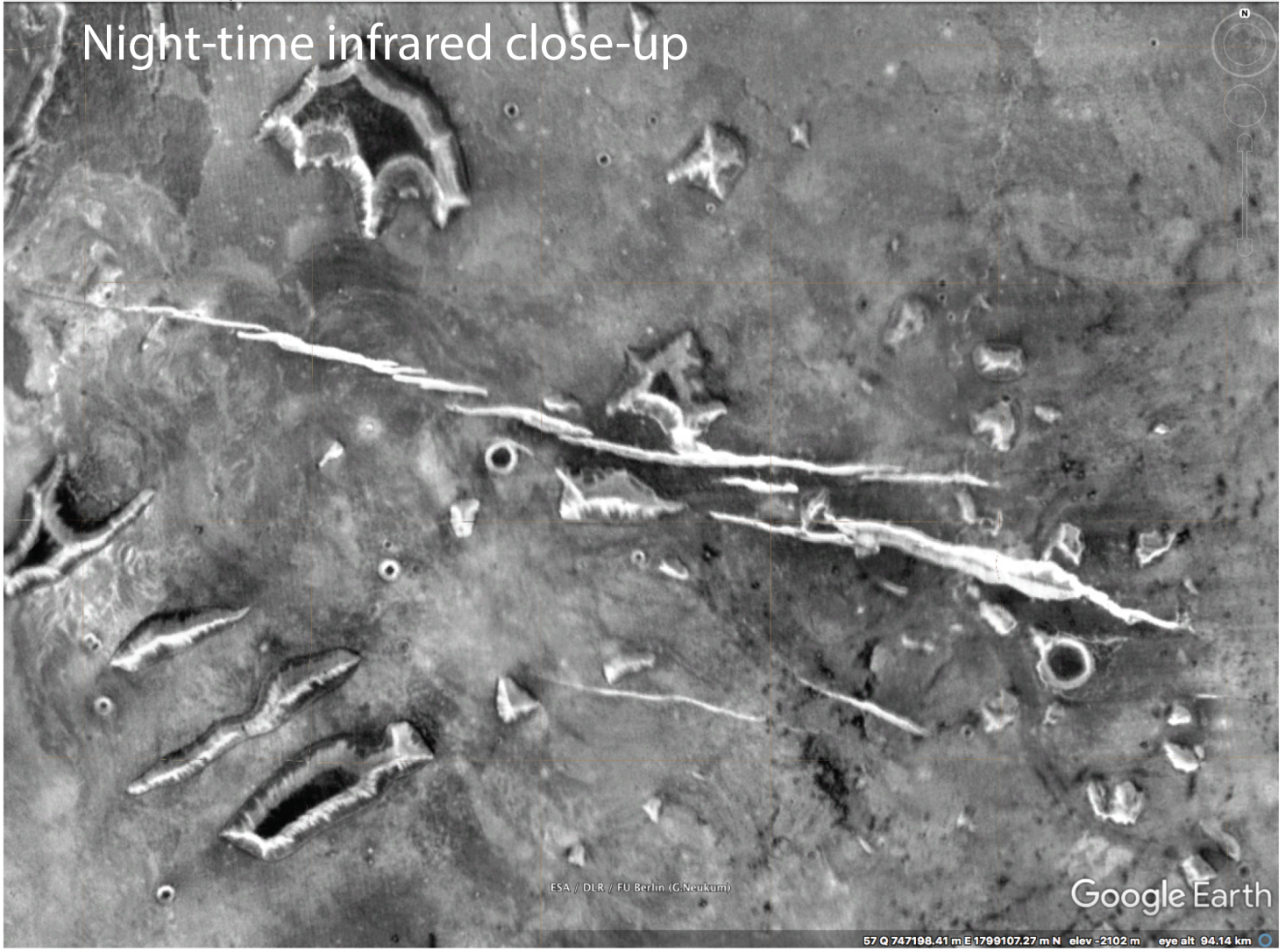

Supplementary Figure S3: Relates to the second point for discussion in the Discussion section of our paper, *2) The effect of local differences lithology and hence weathering/erosion*. The idea that particular lithologies are prone to more or less erosion and as such may control the number and sizes of boulders released from slopes along the graben. S3 a is a close-up night-time infra-red image from THEMIS (Thermal Emission Imaging System) and shows that there is no obvious change in the lithology of rocks forming the graben walls, highlighting only that the graben walls appear to be formed of bedrock.

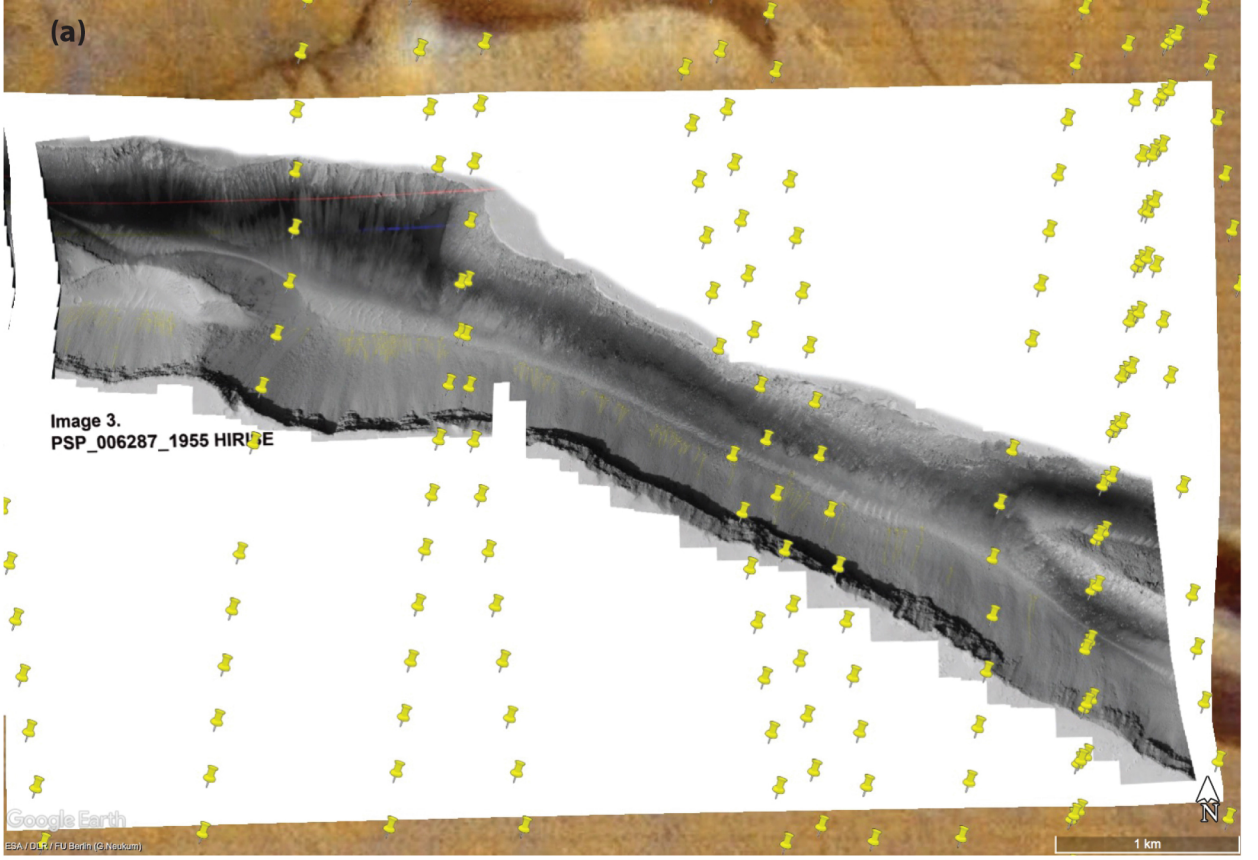

(a) MOLA spacing on HiRISE image

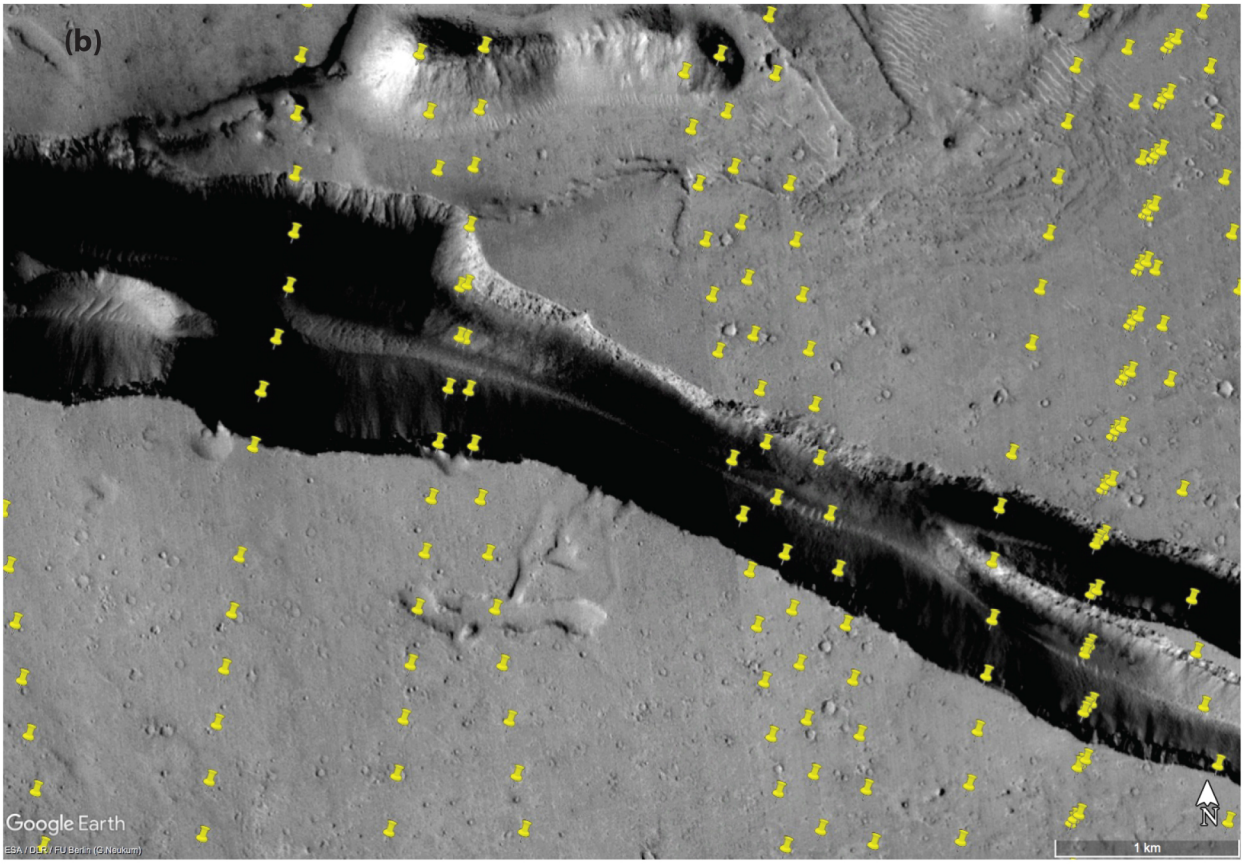

(b) MOLA spacing on CTX image

Supplementary Figure S4: Relates to the third point for discussion in the Discussion section of our paper, *3) Higher cliffs could supply more boulders*. Given that MOLA spot spacing is too coarse (~300 m), measuring the heights and slopes of individual cliffs or talus cones is not possible. S4 (a) (top) shows MOLA spacing on HiRISE image. S4 (b) (bottom) shows MOLA spacing on CTX image.

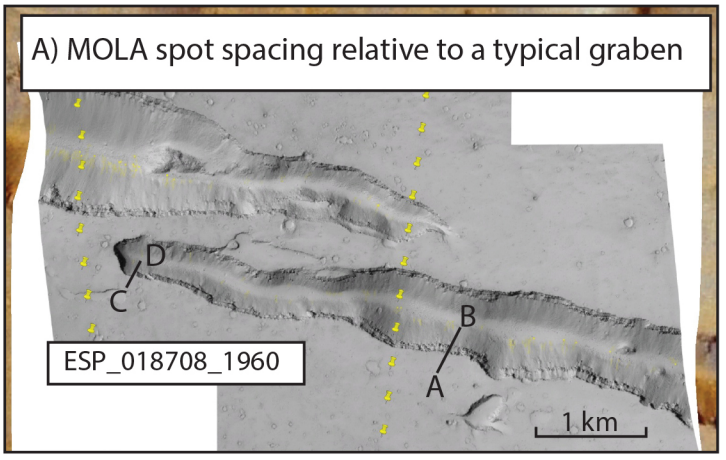

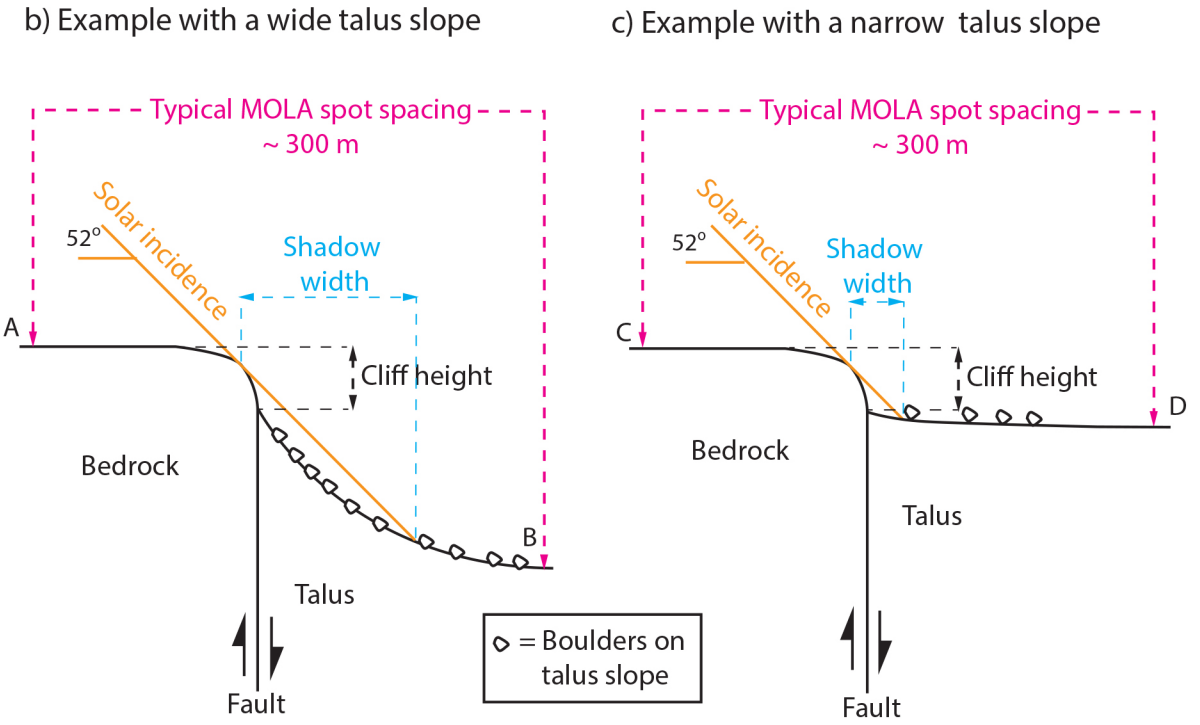

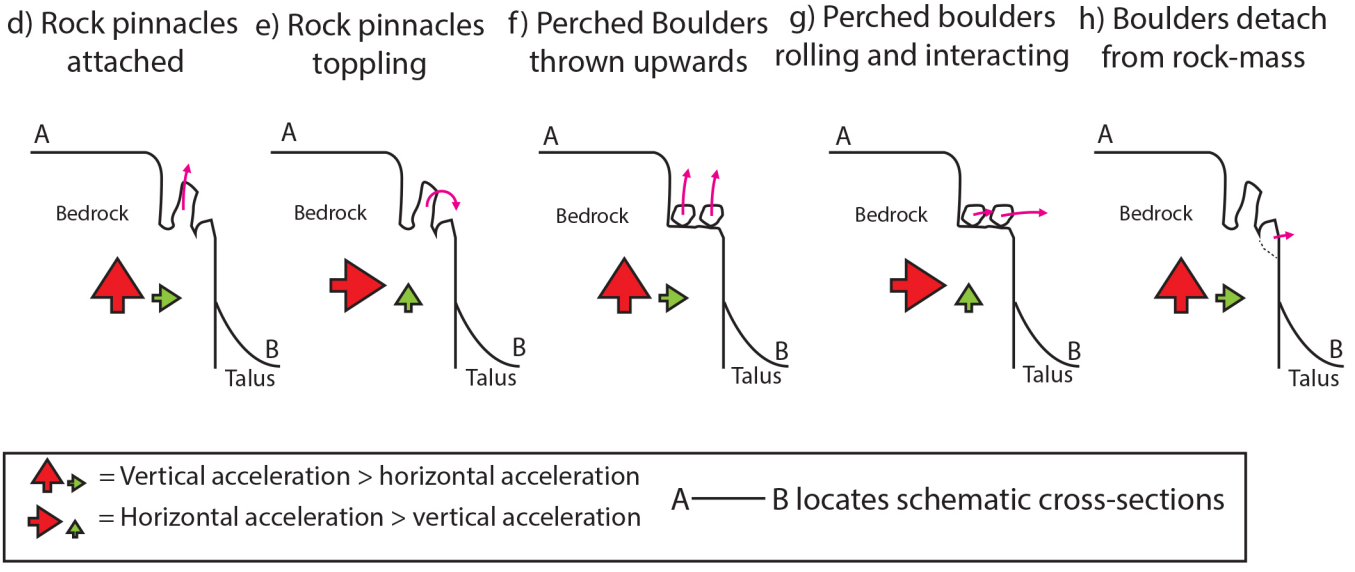

Supplementary Figure S5: Relates to the third point for discussion in the Discussion section of our paper, 3) Higher cliffs could supply more boulders and part of the conclusion to our Discussion section related to horizontal or vertical acceleration mobilizing boulders. S5 b and c are diagrams used to illustrate how shadow width and solar incidence angle cannot be used to define vertical height differences via trigonometry, because the horizontal extents of talus slopes vary between different examples. S5 d through h diagrams are to show how weak gravity on Mars may mean that less force is need to mobilize boulders, but it is hard to be precise as this depends on how each boulder was attached and detached, and whether each boulder was mobilized by vertical or horizontal accelerations.

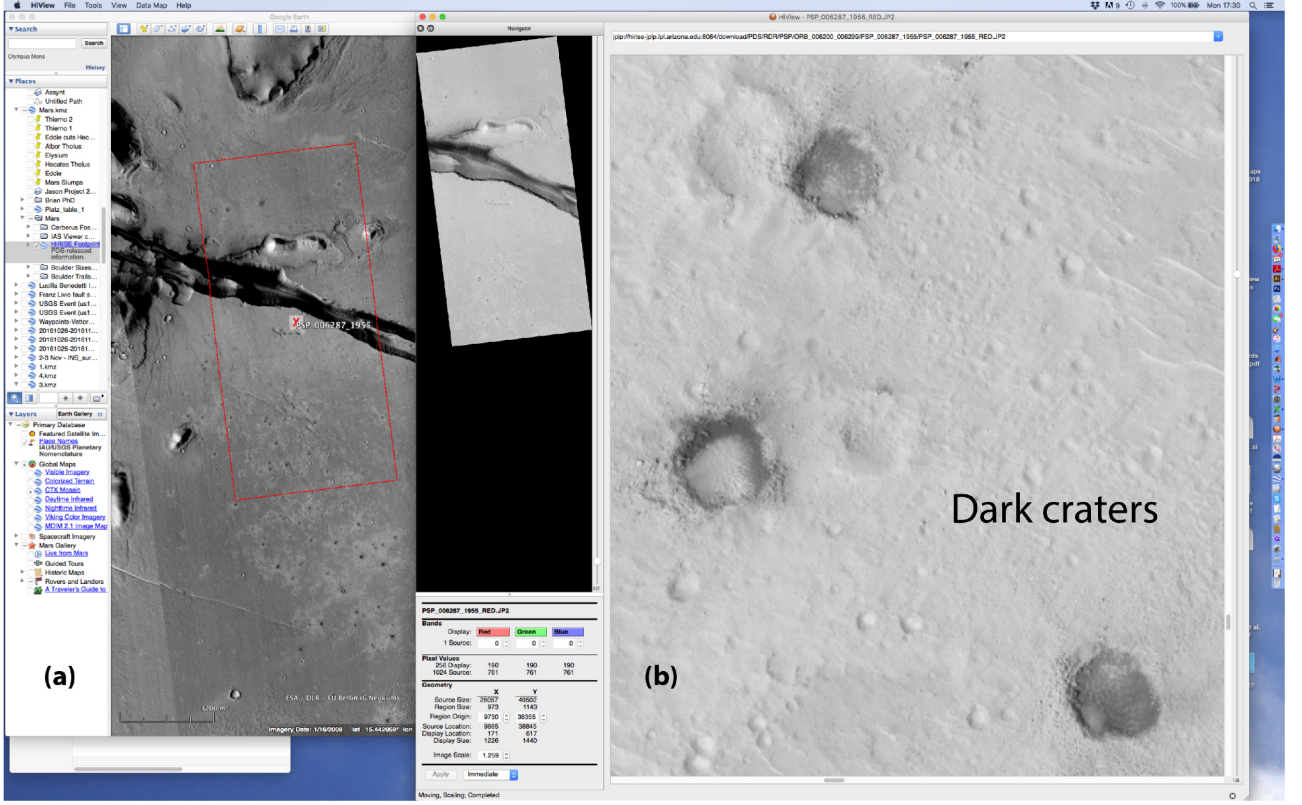

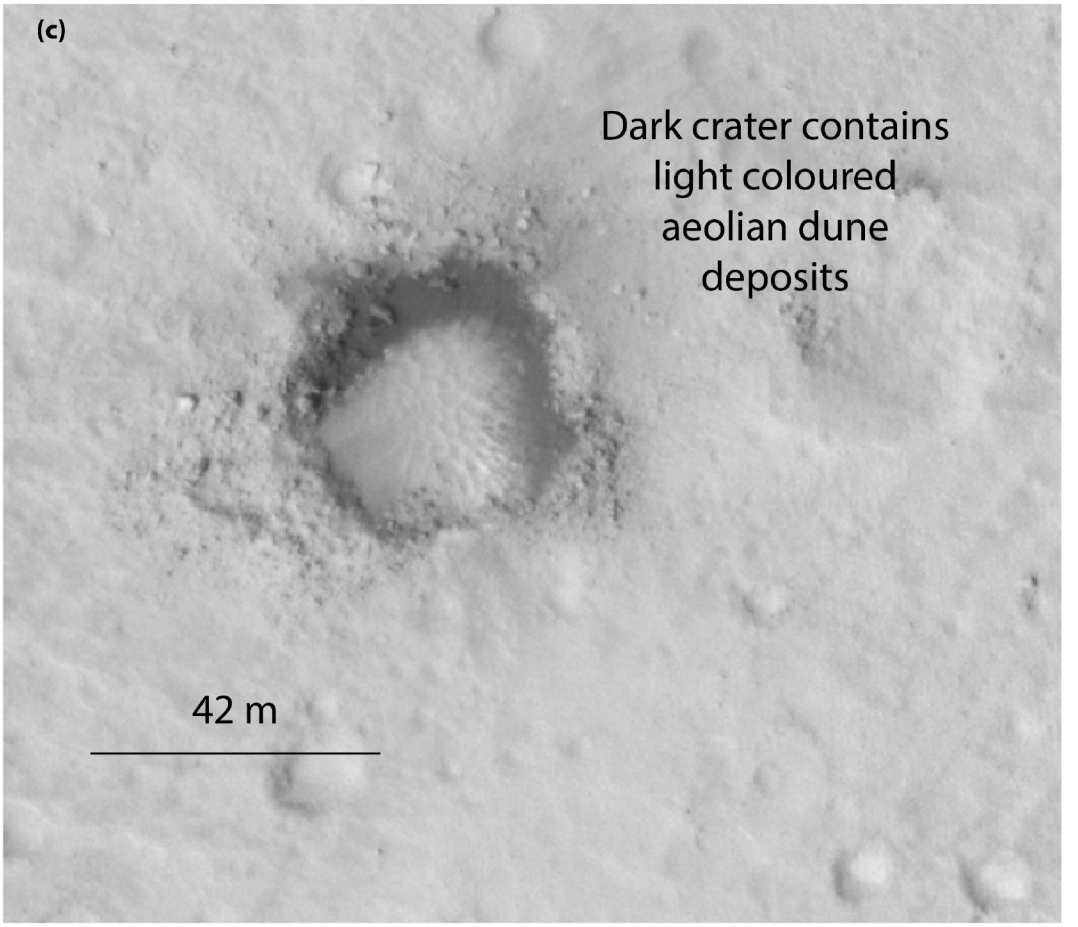

Supplementary Figure S6: Relates to the fourth point for discussion in the Discussion section of our paper, *4) Boulder mobilization caused by nearby impacts.* Although some craters near the anomalies appear dark (S6 a & b), and hence perhaps young, when viewed close up (S6 c) they contain dunes indicating that significant aeolian sedimentation has occurred after their formation, indicating they are probably older than the boulder trails which have not been obscured by aeolian processes. S6 a shows the location of the crater in S6 b and c.

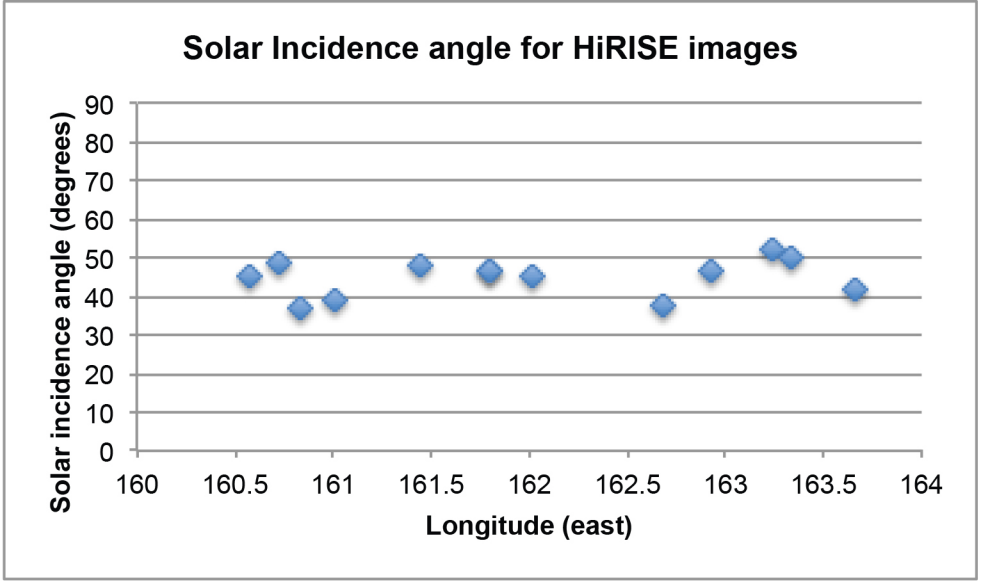

Supplementary Figure S7: Relates to the sixth point for discussion in the Discussion section of our paper, 6) Variation in incidence angle of the images makes trails difficult to see. The solar incidence angles for images studied in our paper are similar, as the graph in S7 shows.

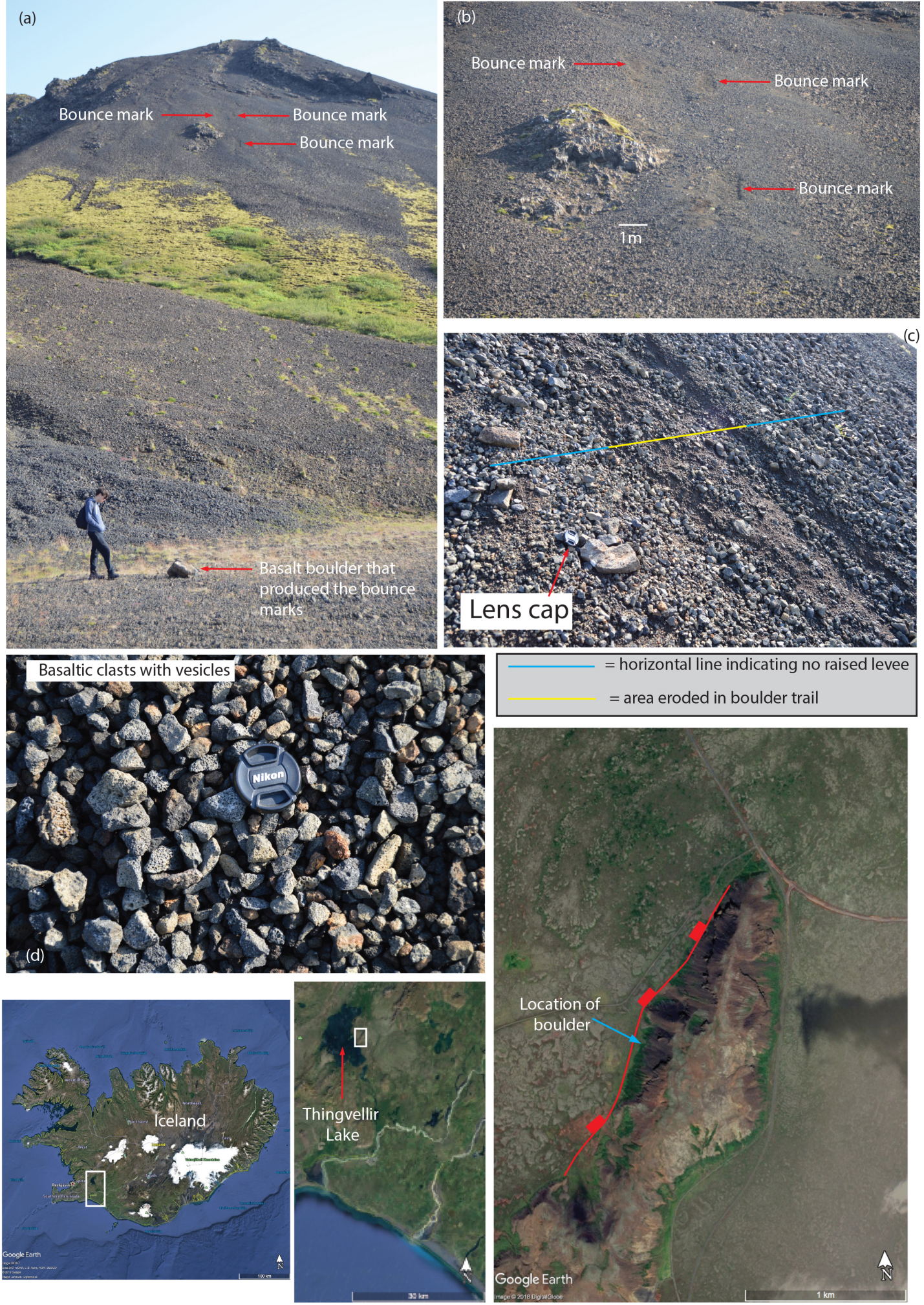

Supplementary Figure S8: Relates to the seventh point for discussion in our Discussion section, *7) The accumulation of boulder trail populations may have developed from multiple single rock falls through time*. Boulder trail examples in Iceland lack raised levees, due to the relatively coarse grain-size. As such, we interpret the grainsize for the examples from Mars as dust to coarse sand. S8 (a), (b), (c) and (d) show boulder trail, bounce marks and boulder. Figures S 8 (e), (f) and (g) are location maps of the boulder trail in S8 (a), (b) and (c).

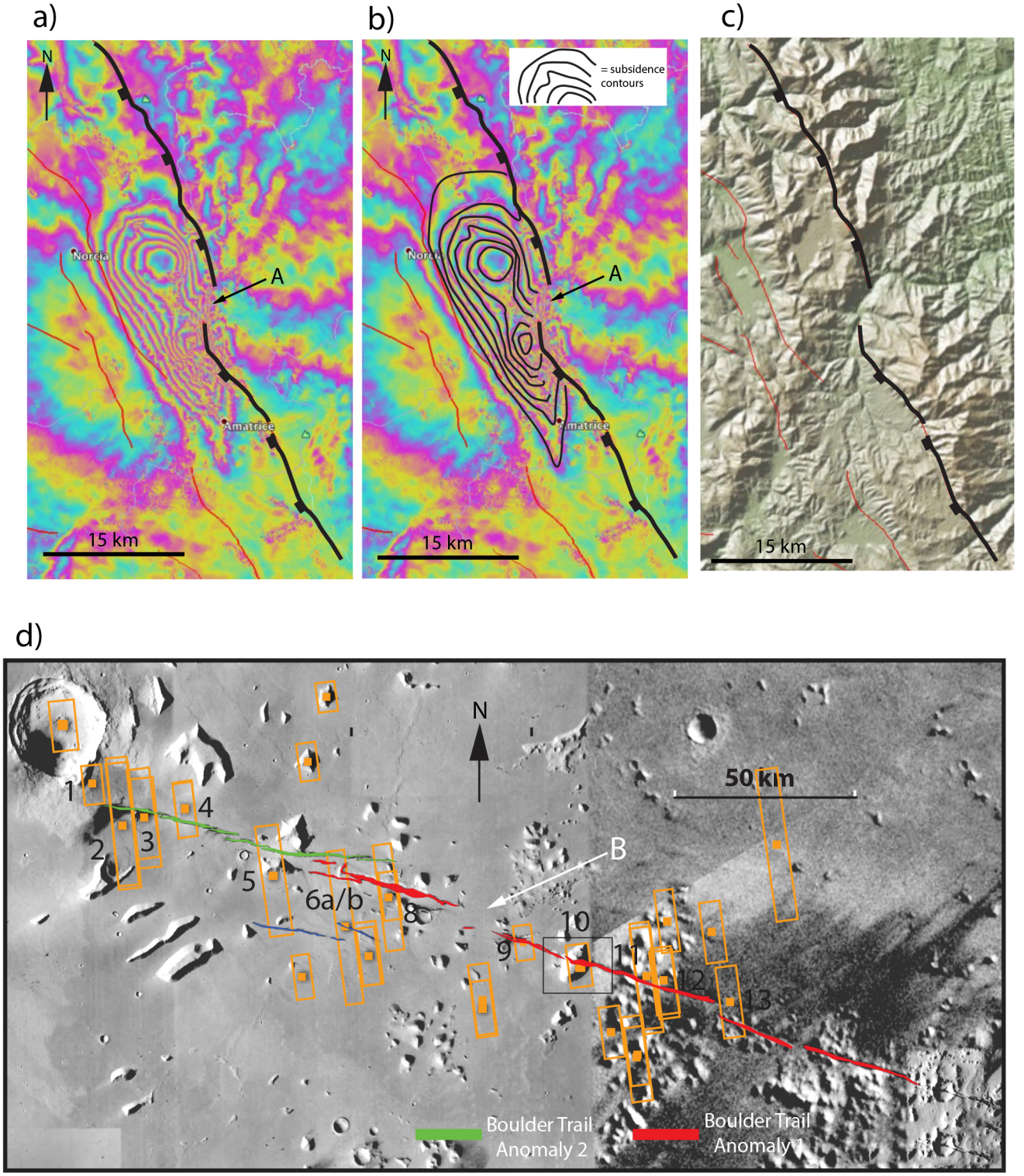

Supplementary Figure S9. (a) and (b) are InSAR data showing the 24th August Mw 6.2 earthquake in central Italy jumping across an area where no surface faulting was reported in the earthquake or on geological maps recording longer term deformation (A), with (c) showing the landscape using an SRTM DEM. This is analogous to the proposed scenario from the fault system in Grjota Valles, (d) where no surface faulting exists on a flat plain (B). InSAR data from http://comet.nerc.ac.uk/latest-earth-quakes-and-eruptions/apennines-earthquakes-aftershocks-italy/ distributed as a kmz file, with one fringe equal to 4.8 cm change in line of sight.